Selected Topics on Space-Charge Effects in Intense Beams*

Steven M. Lund
Lawrence Livermore National Laboratory (LLNL)

The Heavy Ion Fusion Science Virtual National Laboratory

Center for Beam Physics Seminar
Berkeley, CA
13 December 2012

* Supported by the US Dept. of Energy at LLNL and LBNL under contract Nos. DE-AC52-07NA27344 and DE-AC03-76SF0098

Outline

Selected Topics on Space-Charge Effects in Intense Beams

1) US Particle Accelerator School and UC Berkeley courses on "Beam Physics with Intense Space-Charge"

2) Theory and numerical simulations on optimal Einzel lens transport

3) Multipole expansion for realistic modeling of focusing optics

4) Space-Charge induced transport limits in quadrupole focusing channels

5) Nonlinear focusing channel for stable beam transport and possible application to NGLS/APEX

Accelerator school courses taught for 10+ years on
"Beam Physics with Intense Space-Charge"
have been influential in educating a generation of research specialists and material developed for course relevant to many contemporary research problems which cannot be found in other sources.

- Taught jointly by J.J. Barnard (Longitudinal) and S.M. Lund (Transverse)

- Semester course equivalents given at:
  - 5X: US Particle Accelerator School
  - 1X: UC Berkeley Nuclear Engineering Deptartment
  - 1X: LBNL (Simulations)

- Course web page (last 2011 version; next 2013) archives notes:
  http://hifweb.lbl.gov/USPAS_2011/

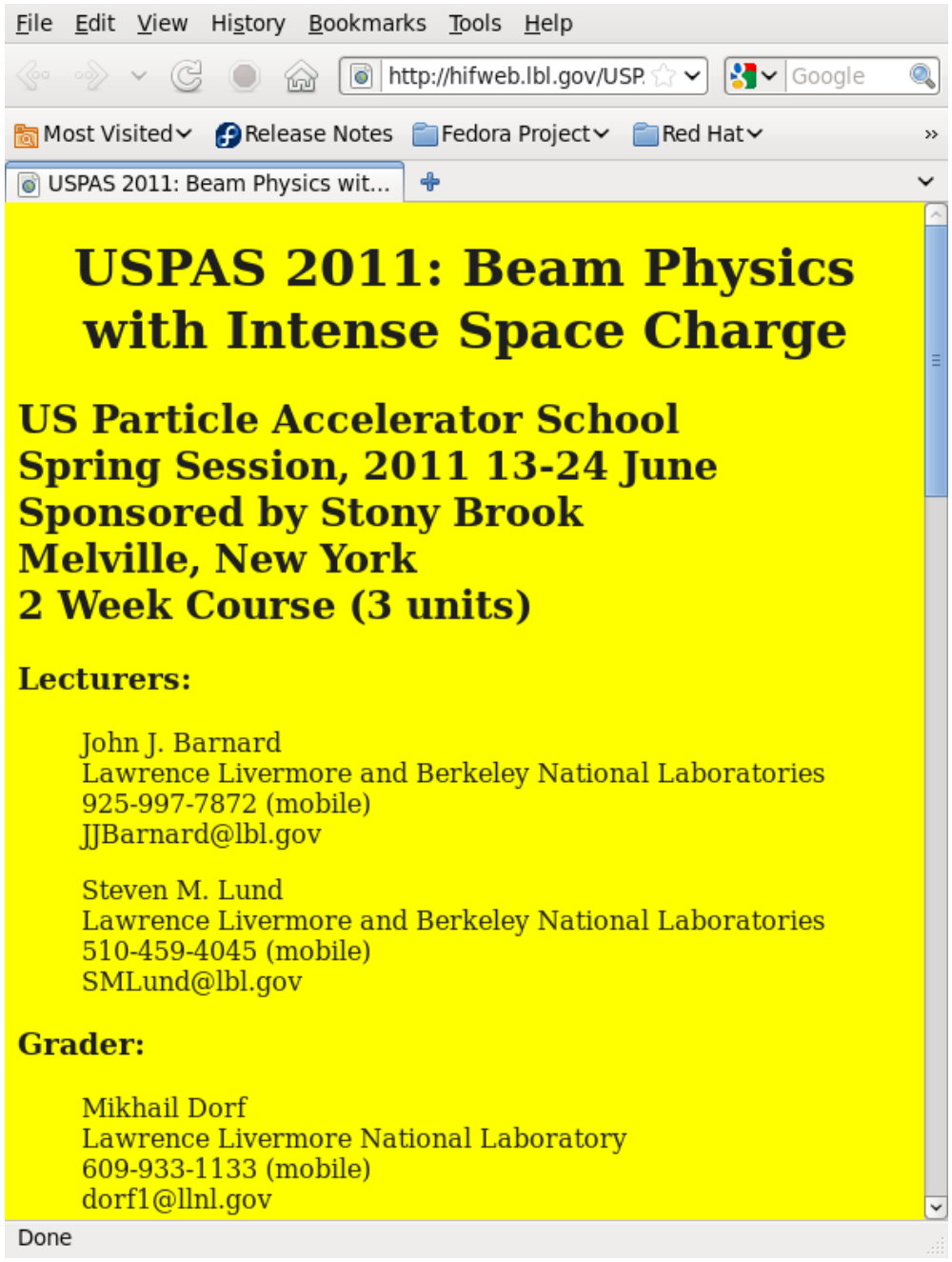

http://hifweb.lbl.gov/USPAS_2011/

Cource Details:

Extended Overview (pdf)
Full Topical Outline (pdf)

Lecture Notes:

Lecture notes will be periodically posted on this web site before material is covered in class. Paper copies of lecture notes will also be handed out in class. Corrections and additions may also be posted on the web site subsequent to lectures. Material is organized by topic in the rough order intended to be covered in class. Postings will be in pdf format including scans of handwritten notes, and conversions of electronic slides produced in OpenOffice and Microsoft PowerPoint.

• J.J. Barnard	Introduction, Envelope Equations, and Current Limits
• S.M. Lund	Transverse Particle Dynamics
• S.M. Lund	Transverse Equilibrium Distribution Functions
• S.M. Lund	Transverse Particle Resonances with Applications to Circular Accelerators
• J.J. Barnard	Injectors and Longitudinal Physics
• J.J. Barnard	Continuous Focusing Beam Envelope Modes and Halo
• S.M. Lund	Transverse Centroid and Envelope Descriptions of Beam Evolution
• S.M. Lund	Transverse Kinetic Stability
• J.J. Barnard	Pressure, Scattering, and Electron Effects
• J.J. Barnard	Final Focusing and Example Applications of Intense Beams
• S.M. Lund	Numerical Simulations
• J.J. Barnard	Barnard Lectures Summary

Selected Topics on Space-Charge Effects in Intense Beams

1) US Particle Accelerator School and UC Berkeley courses on "Beam Physics with Intense Space-Charge"

2) Theory and numerical simulations on optimal Einzel lens transport

3) Multipole expansion for realistic modeling of focusing optics

4) Space-Charge induced transport limits in quadrupole focusing channels

5) Nonlinear focusing channel for stable beam transport and possible application to NGLS/APEX

Geometry for Periodic Stacked Washer Einzel Lens

Unipolar, Thin Washer

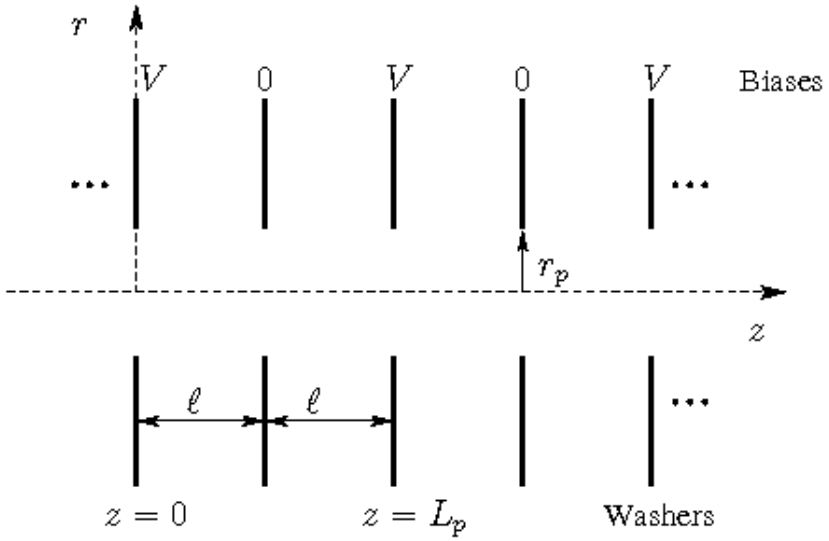

Thick Washer Replacement

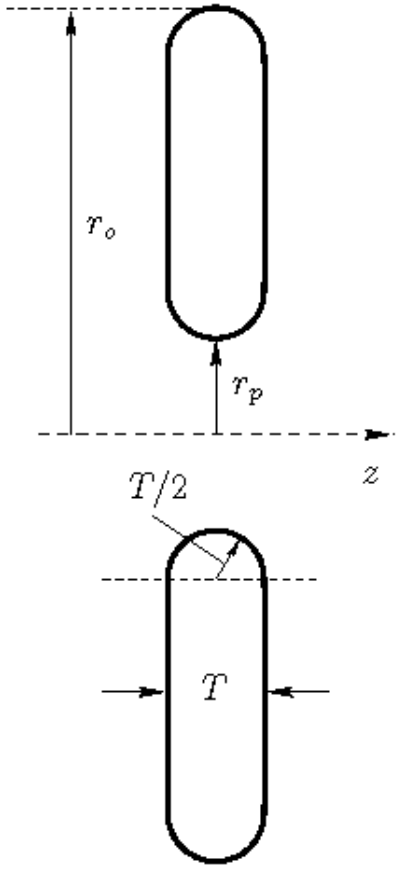

Bipolar, Thin Washer

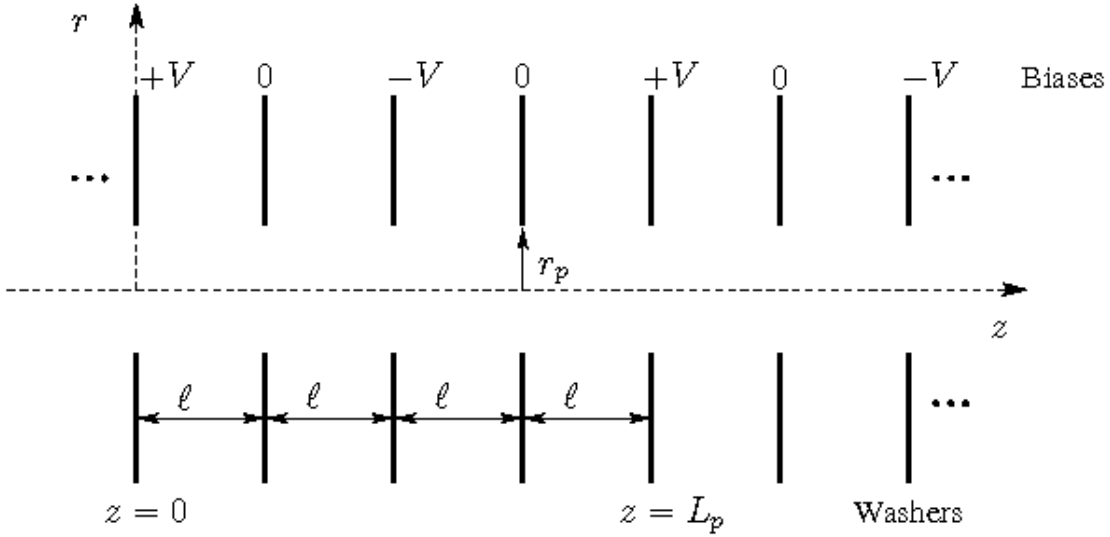

Lattice Period:

$$L_p = \begin{cases} 2\ell, & \text{Unipolar} \\ 4\ell, & \text{Bipolar} \end{cases}$$

Applied Fields: Need simple, accurate model to optimize

Laplace Equation for electrostatic field:

$$\left(\frac{\partial^2}{\partial r^2}+\frac{1}{r}\frac{\partial}{\partial r}+\frac{\partial^2}{\partial z^2}\right)\phi(r,z)=0$$

$$\phi(r,z)=\text{const on washers}$$

Washer potential solved in sclaed geometry using Warp code:

Unipolar $r_p/\ell=1$ Bipolar

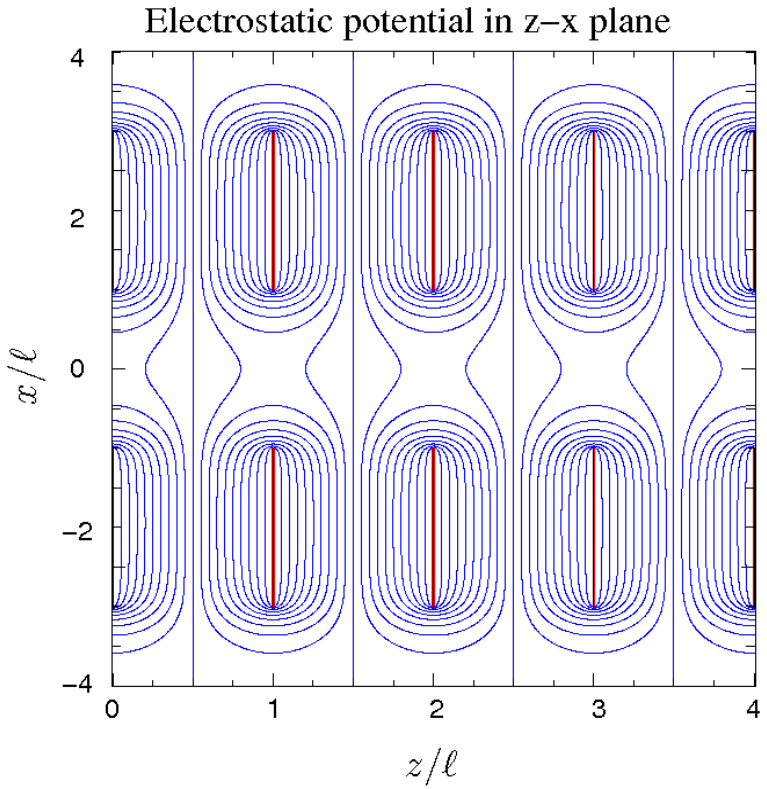

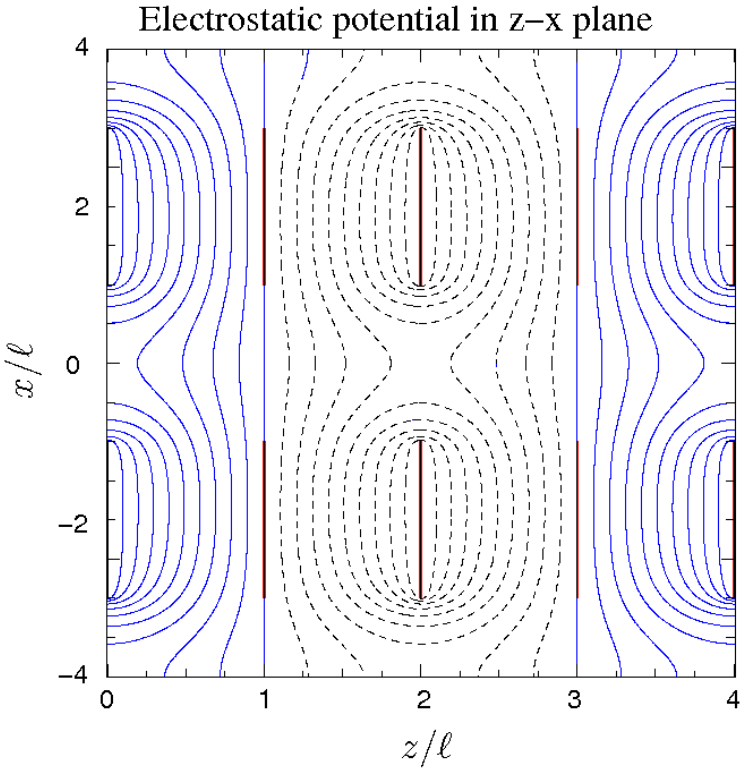

Analytical Field Model

Expand potential as:

$$\phi(r,z) = \sum_{\nu=0,1,\cdots}^{\infty} \frac{(-1)^\nu}{2^{2\nu}(\nu!)^2} \frac{\partial^{2\nu}}{\partial^{2\nu} z} \phi_0(z) r^{2\nu}$$

$$\phi_0(z) \equiv \phi(r=0,z) = \text{on-axis potential}$$

Linear fields from leading-order terms:

$$\mathbf{E}_\perp = -\frac{\partial}{\partial \mathbf{x}_\perp}\phi \simeq \frac{1}{2}\frac{\partial^2 \phi_0}{\partial z^2}(\hat{\mathbf{x}}x + \hat{\mathbf{y}}y)$$

$$E_z = -\frac{\partial}{\partial z}\phi \simeq -\frac{\partial \phi_0}{\partial z}$$

Approximate Model for On-Axis Potential

Ordinary differential equation:

$$\frac{\partial^2}{\partial z^2}\phi_0(z) - \frac{4}{r_p^2}\phi_0(z) \simeq -\frac{4}{r_p^2}\phi(r = r_p, z)$$

$$\phi(r = r_p, z) = \text{Potential at Aperture}$$

Expand the aperture potential in a periodic Fourier series:

$$\phi(r = r_p, z) = V \sum_{n=0,1,3,\cdots}^{\infty} f_n \cos\left(\frac{2\pi n z}{L_p}\right)$$

f_n = Fourier Coefficients $\qquad f_n = f_n(r_p/\ell)$

Periodic solution:

$$\phi_0(z) = V \sum_{n=0,1,3,\cdots}^{\infty} \frac{f_n}{1 + (n\pi r_p/L_p)^2} \cos\left(\frac{2\pi n z}{L_p}\right)$$

Symmetry relations connecting unipolar and bipolar solutions shows that:

$$f_0\left(\frac{r_p}{\ell}\right) = \begin{cases} \frac{1}{2}, & \text{Unipolar} \\ 0, & \text{Bipolar} \end{cases} \qquad f_n\left(\frac{r_p}{\ell}\right) = \begin{cases} g_n\left(\frac{r_p}{\ell}\right), & \text{Unipolar} \\ 2g_n\left(\frac{1}{2}\frac{r_p}{\ell}\right), & \text{Bipolar} \end{cases}$$

g_n = common coefficient function

Data from parametric Warp numerical field solutions and nonlinear numerical curve fitting show that the harmonic coefficients are well fit by:

- Thin washers
- Large radial extent washers

$$g_n = c_{n,1} \exp\left[-c_{n,2}(r_p/\ell)^2\right]$$

n	$c_{n,1}$	$c_{n,2}$
1	0.3891	0.5823
3	0.04873	4.740
5	0.01846	12.85
7	0.009738	24.88

Only 8 numbers to describe first harmonics up to n = 8 !

Linear field model is extremely accurate over a wide range of geometric aspect ratios for both unipolar and bipolar systems

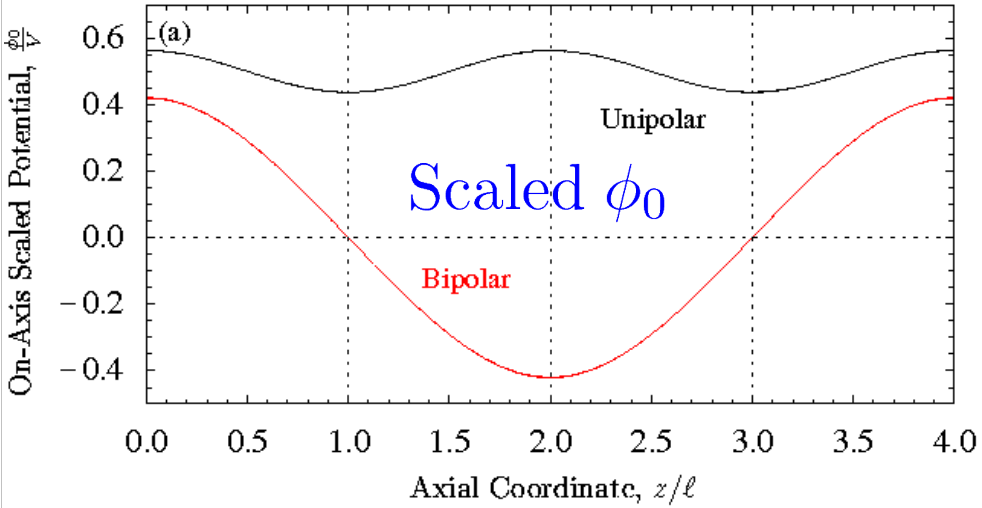

Results for aspect ratio

$r_p/\ell = 1$

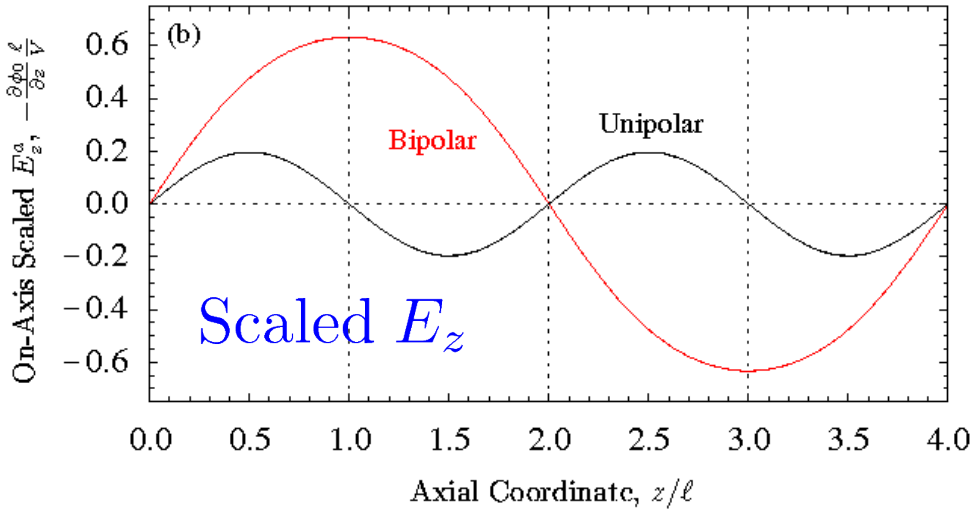

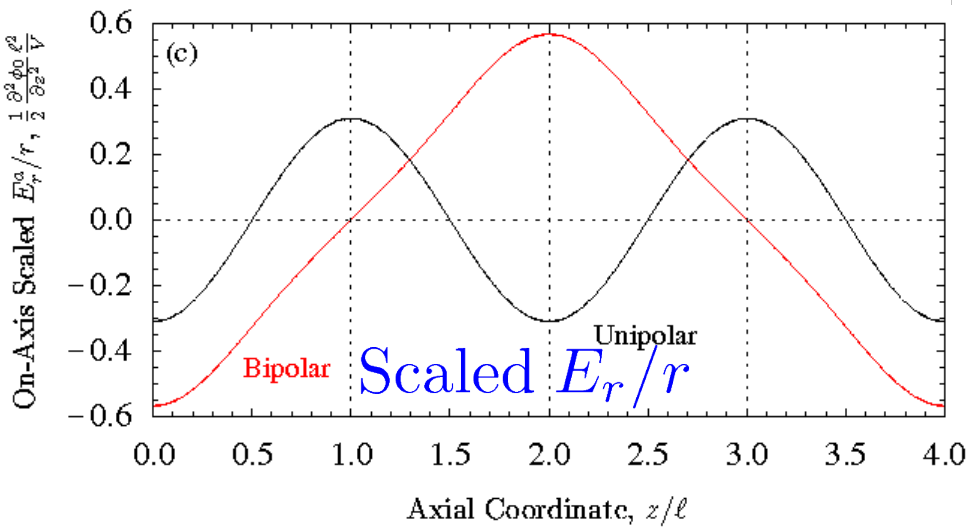

WARP solution (dashed curves) almost exactly overlays reduced field model with fit coefficients (solid curves)!

- Reduced model sets scale of potential oscillation – needed for correct design limits!
- Reduced model accuracy enables accurate envelope models without full simulation

Radial extent of Einzel lens system can be modest without significantly attenuating linear field strength

Smaller radial extent allows:

- Compact radial structures
- Clearance for voltage holding

For optimum linear focusing aspect ratio r_p/ℓ and thin washers:

Linear Field Variation

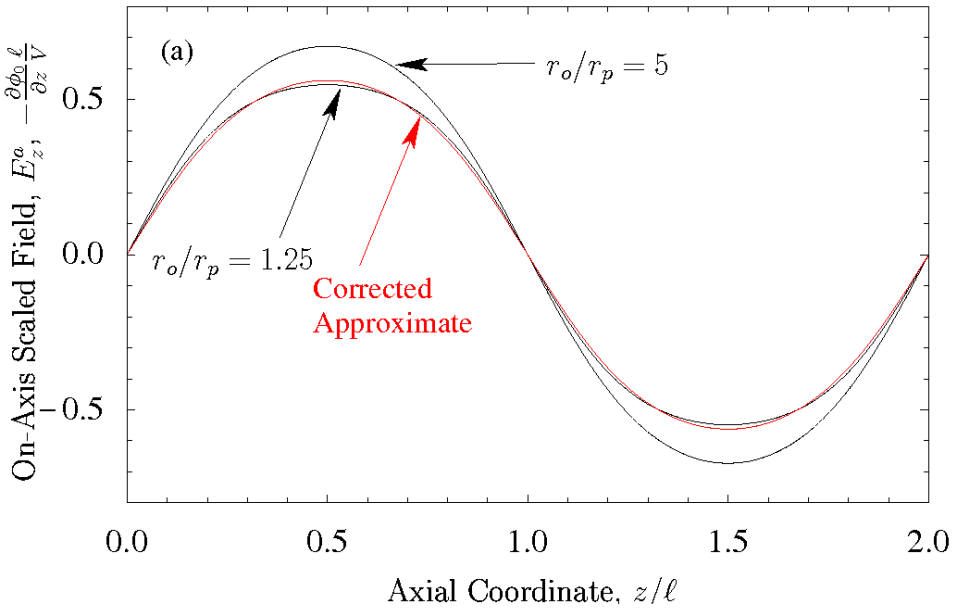

Harmonic Correction Factor

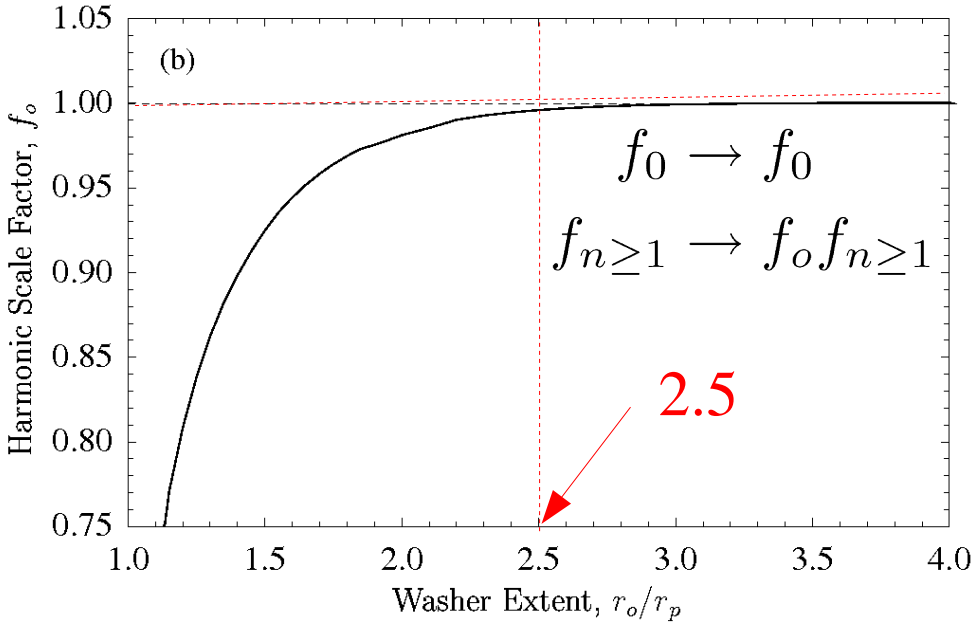

Washer extents with $r_o/r_p = 2.5$ should be sufficient for most applications

Peak field always occurs at outer radial edge of washer and required thickness can be read off scaling curves

Field Intensity

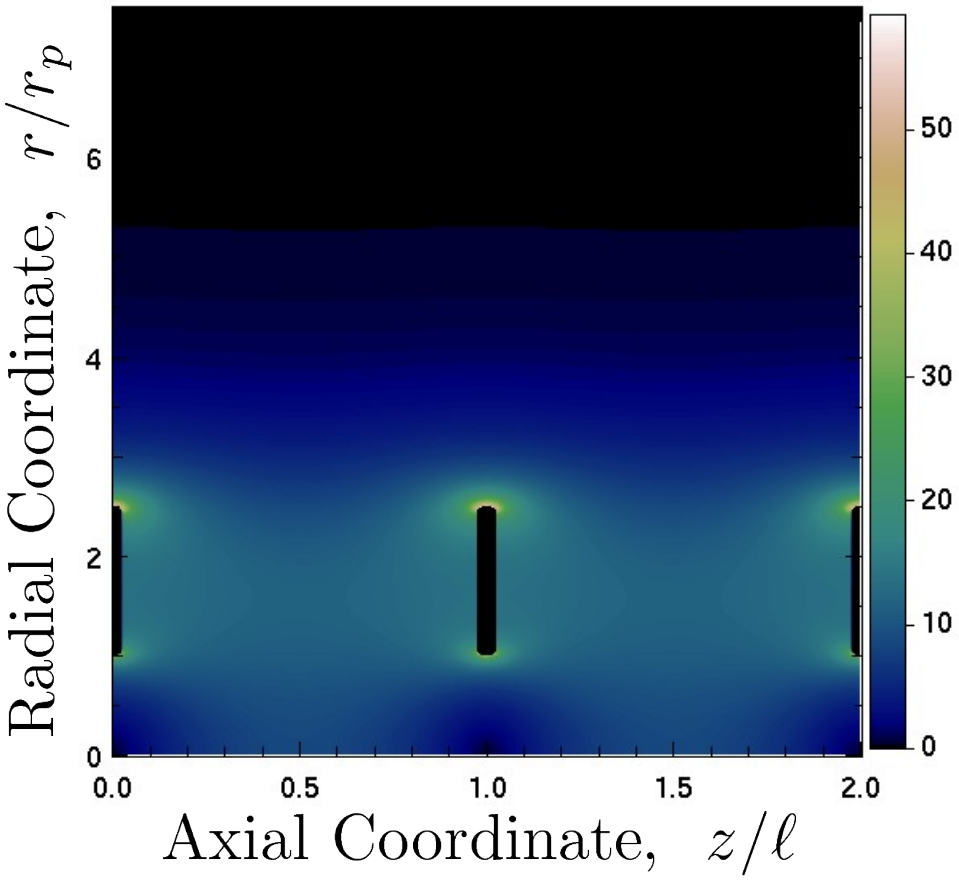

Max Field Scaling

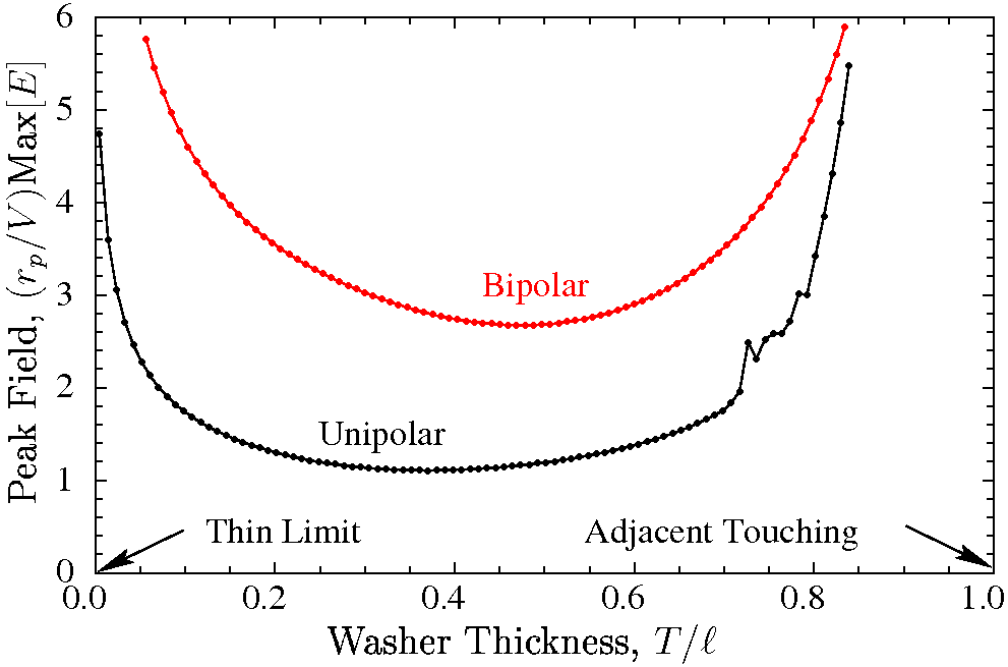

Field strength scaling curves apply to systems with

- Optimal aspect ratio r_p/ℓ
- Outer radial washer extent $r_o/r_p = 2.5$

Plate thickness and radiusing edges of biased washers necessary to limit peak fields and suppress breakdown

Voltage holding scaling for distances $d \gtrsim 1$ cm under vacuum conditions characteristic of our classes of machines:

$$E \lesssim 100 \frac{\text{kV}}{\text{cm}} \sqrt{\frac{1 \text{ cm}}{d}}$$

A, Faltens, *Handbook Accel. Phys.*

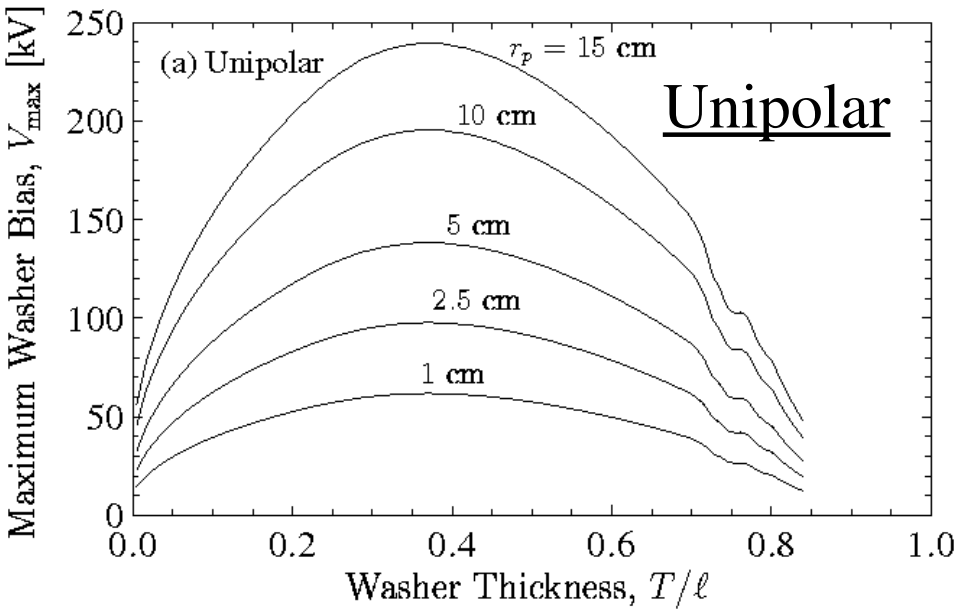

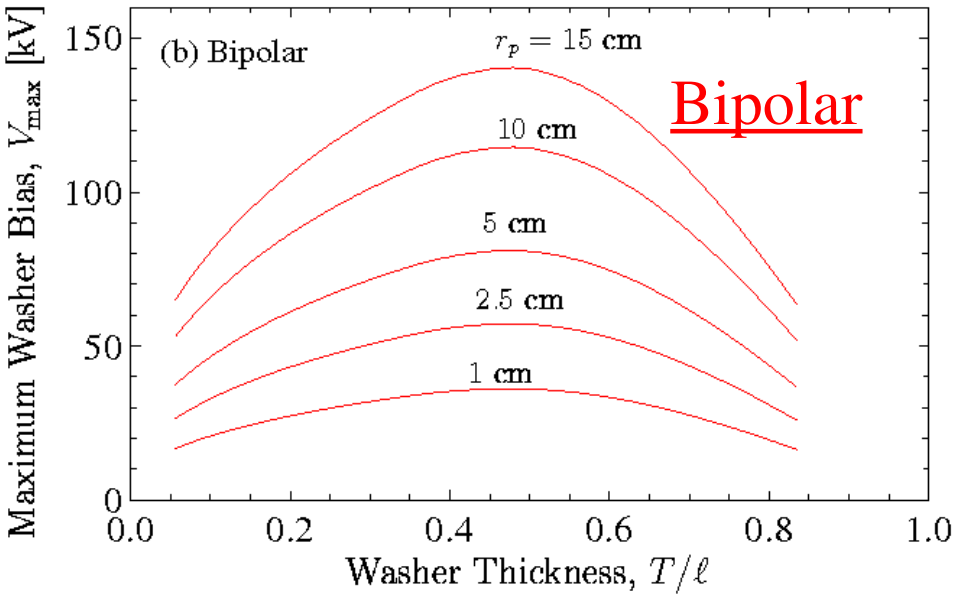

Nonlinear fields can be large at high aperture fill factor

WARP used to contour axial and radial nonlinear fields as fractions of linear focusing values

- Shown for optimum linear focusing aspect ratio r_p/ℓ and thin washers
- Applies to both unipolar and bipolar systems

Axial Contours: $F_z = \dfrac{E_z^a + \dfrac{\partial \phi_0}{\partial z}}{-\dfrac{\partial \phi_0}{\partial z}}$

Radial Contours: $F_r = \dfrac{E_r^a - \dfrac{1}{2}\dfrac{\partial^2 \phi_0}{\partial z^2} r}{\dfrac{1}{2}\dfrac{\partial^2 \phi_0}{\partial z^2} r}$

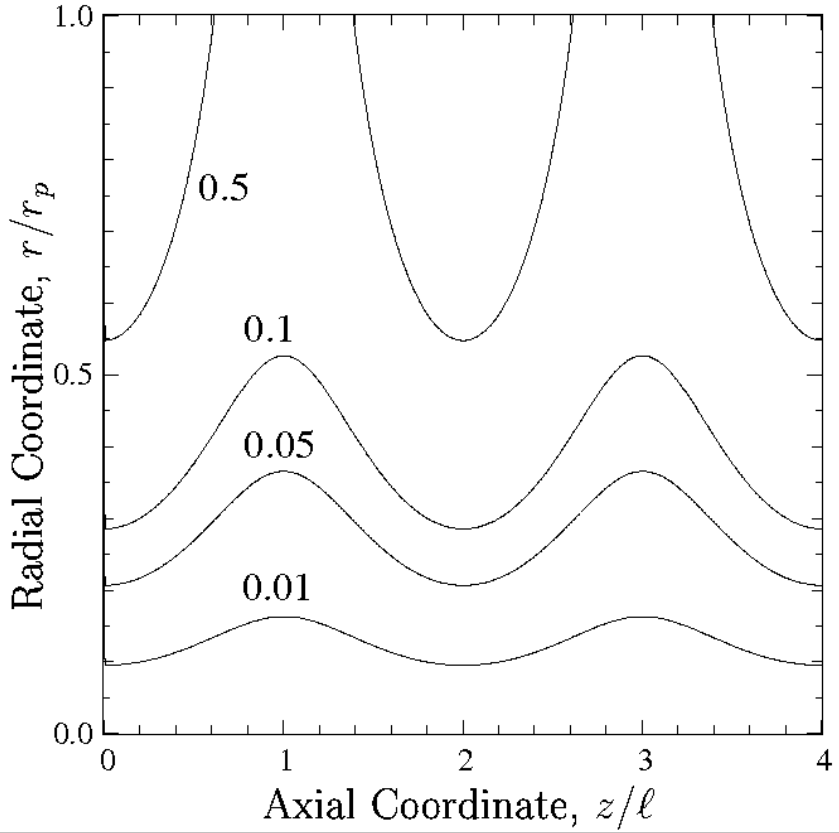

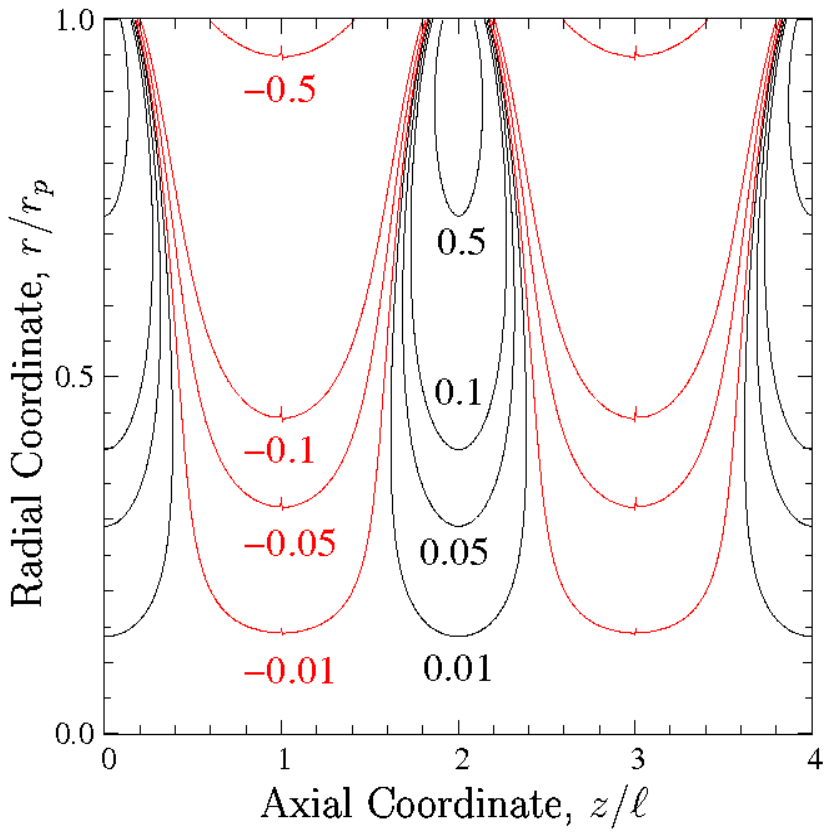

Linear Transverse Dynamics

Transverse equation of motion for a particle moving within a uniform density beam with radius $R(z)$ without applied axial compression:

$$\mathbf{x}_\perp'' - \frac{1/2}{1-\Phi}\frac{\partial \Phi}{\partial z}\mathbf{x}_\perp' - \frac{1/4}{1-\Phi}\frac{\partial^2 \Phi}{\partial z^2}\mathbf{x}_\perp - \frac{1}{(1-\Phi)^{3/2}}\frac{Q}{R^2}\mathbf{x}_\perp = 0$$

$$\Phi \equiv \frac{q\phi_0}{\mathcal{E}_b} = \frac{\text{Particle Potential Energy}}{\text{Particle Total Energy}} \qquad ' \equiv \frac{d}{dz}$$

Incorporates conservation constraints:

$$\frac{1}{2}mv_z^2 + q\phi_0 \equiv \mathcal{E}_b = \text{const}$$ Conservation of total longitudinal energy

$$I \equiv v_z\lambda = \text{const}$$ Conservation of current: continuity eqn

and a consistent definition of the perveance Q which reduces to the usual form axially outside the Einzel lens system: $\phi_0 = 0 \Leftrightarrow \Phi = 0$

$$Q \equiv \frac{qI}{2^{5/2}\pi\epsilon_0\mathcal{E}_b^{3/2}/m^{1/2}} = \frac{qI}{2\pi\epsilon_0 m(2\mathcal{E}_b/m)^{3/2}} = \text{const}$$

Transform to "normalized coordinates" simplifies dynamical description

Introduce transformed "tilde" coordinates

$$\tilde{\mathbf{x}}_\perp = \sqrt{v_z}\mathbf{x}_\perp$$
$$\tilde{\mathbf{x}}'_\perp = \frac{1}{2}\frac{v'_z}{\sqrt{v_z}}\mathbf{x}_\perp + \sqrt{v_z}\mathbf{x}'_\perp$$

$$dx \otimes dx' = \frac{1}{v_z} d\tilde{x} \otimes d\tilde{x}'$$
$$dy \otimes dy' = \frac{1}{v_z} d\tilde{y} \otimes d\tilde{y}'$$

Then the equation of motion has simplified "Hill's Equation" form

$$\tilde{\mathbf{x}}''_\perp + \kappa(z)\tilde{\mathbf{x}}_\perp + \kappa_{sc}(z)\tilde{\mathbf{x}}_\perp = 0$$

$$\kappa(z) \equiv \frac{3}{16}\left(\frac{\partial\Phi/\partial z}{1-\Phi}\right)^2$$ Applied Focusing $$\Phi \equiv \frac{q\phi_0}{\mathcal{E}_b}$$

$$\kappa_{sc}(z) \equiv -\frac{1}{(1-\Phi)^{3/2}}\frac{Q}{R^2}$$ Space-Charge DeFocusing

Form of applied focusing κ shows that Einzel lens always focusing regardless of the sign of bias *V* !

- Positive *V* stronger due to $1-\Phi$ factor in denominator

Optimal geometric aspect ratios can be evaluated for the strongest possible Einzel lens focusing

The largest value of the scaled period average focusing strength

$$r_p^2\overline{\kappa} \equiv r_p^2 \int_{L_p} \frac{dz}{L_p}\, \kappa(z) \qquad \kappa(z) = \frac{3}{16}\left(\frac{\partial\Phi/\partial z}{1-\Phi}\right)^2 \qquad \Phi = \frac{q\phi_0}{\mathcal{E}_b}$$

Provides the strongest possible applied focusing for fixed values of:

$r_p = \text{const}$ Aperture

$qV/\mathcal{E}_b = \text{const}$ Scaled Bias

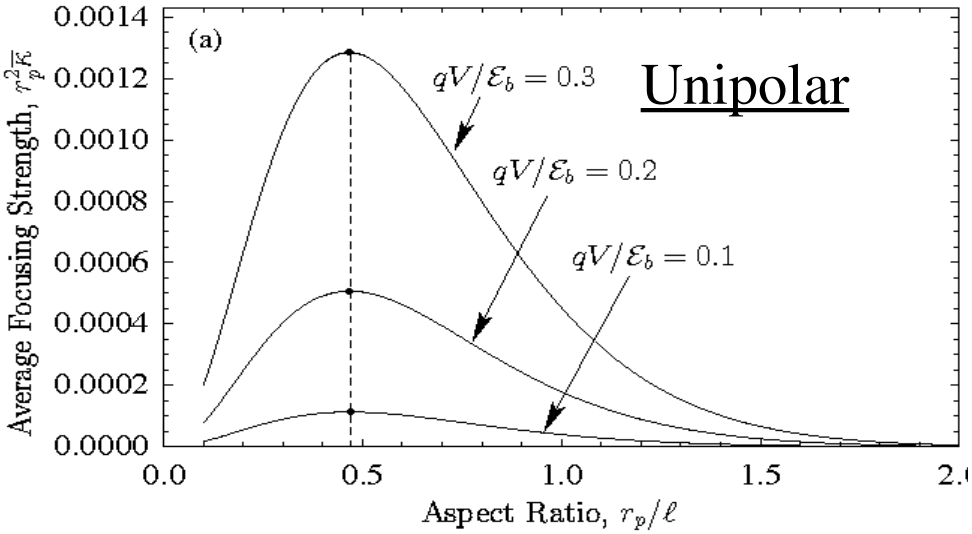

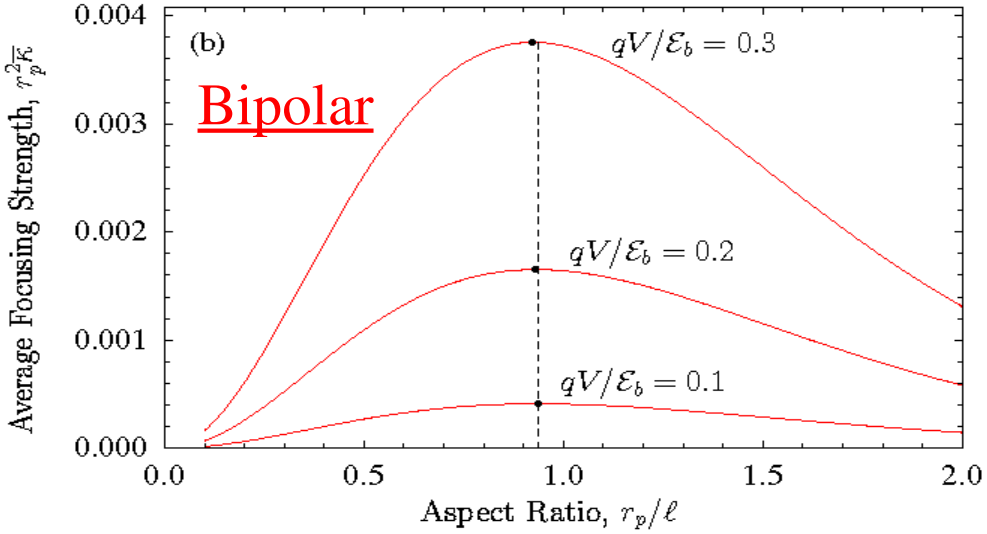

$\frac{r_p}{L_p} = 0.2342$ optimizes both unipolar and bipolar focusing for $\frac{|qV|}{\mathcal{E}_b} \lesssim 0.5$

At optimal aspect ratios

$$\frac{r_p}{L_p} = 0.2344 \quad \Longleftrightarrow \quad \frac{r_p}{\ell} = \begin{cases} 0.4688, & \text{Unipolar} \\ 0.9377, & \text{Bipolar} \end{cases}$$

contrast focusing functions: $\kappa(z) = \frac{3}{16}\left(\frac{\partial\Phi/\partial z}{1-\Phi}\right)^2 \qquad \Phi = \frac{q\phi_0}{\mathcal{E}_b}$

for same values of $qV/\mathcal{E}_b$

Optimized Focusing Strength

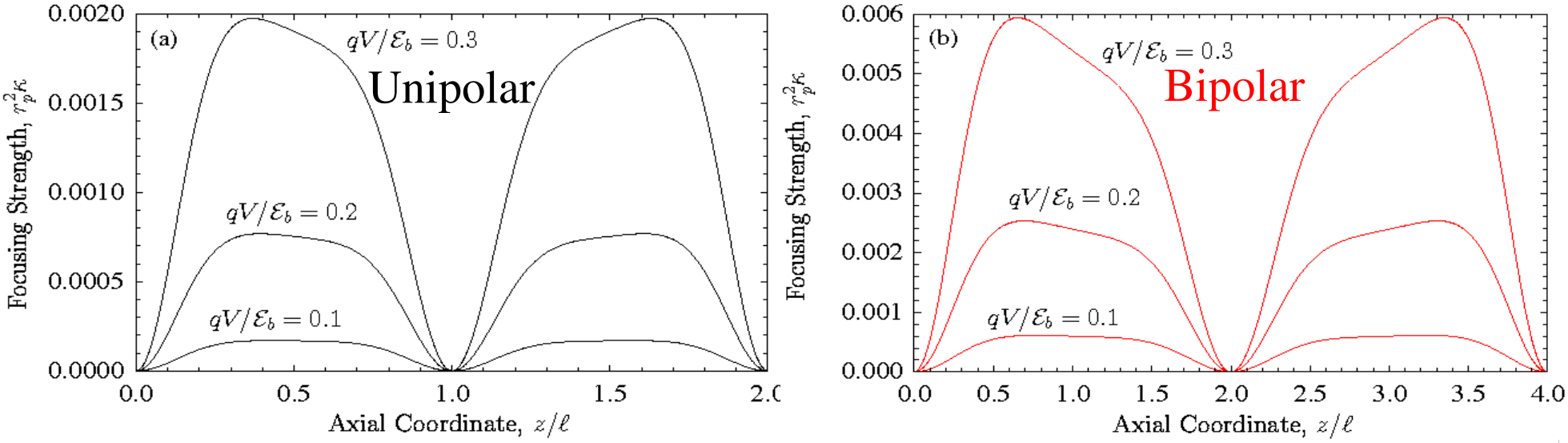

- Stronger focusing for bipolar relative to unipolar for the same values of $qV/\mathcal{E}_b$ yields compact beam sizes
  - Illustrate later with envelope results

Single particle stability for optimized Einzel lens focusing shows that large biases are possible

Phase Advance and Stability Limits: calculated for optimized geometry using a transfer matrix in transformed variables $\frac{1}{2}\left|\mathrm{Tr}\,\tilde{\mathbf{M}}\right| \leq 1 \Longleftrightarrow$ Stability

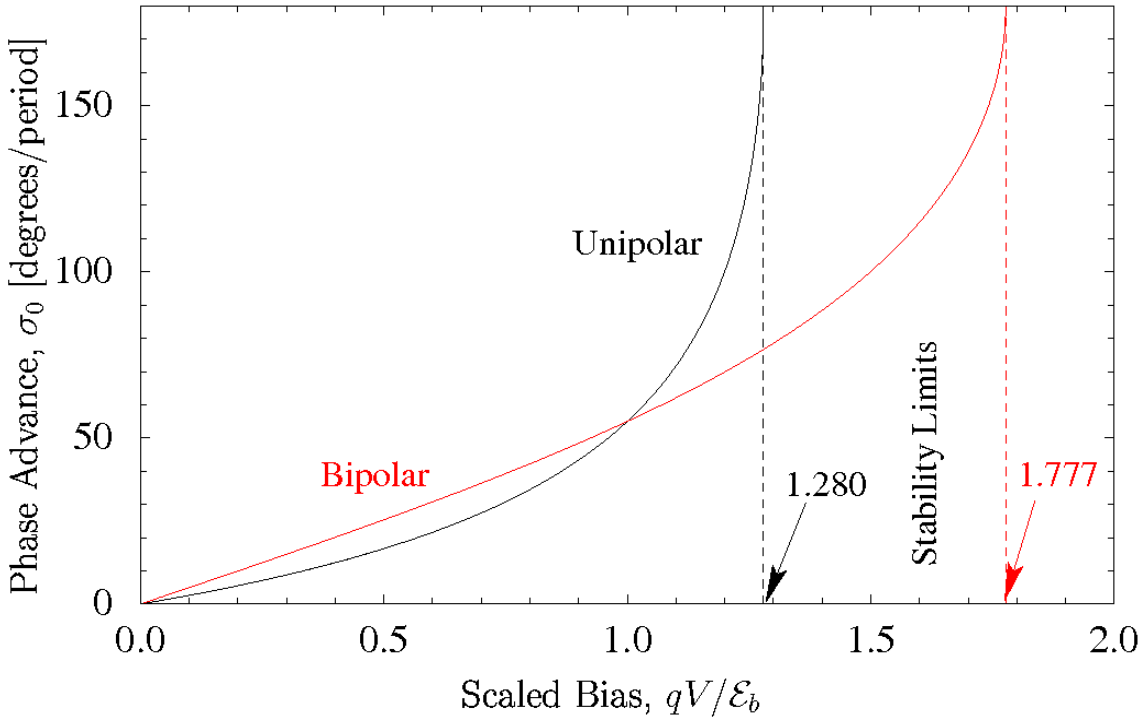

Properties:

- Phase advances very low till near stability limit
- Biases can be significant fraction of beam energy due to low phase advances

$$\Phi = 1 \quad \text{and } v_z = 0 \quad \Longleftrightarrow \quad \frac{qV}{\mathcal{E}_b} = \begin{cases} 1.366, & \text{Unipolar}, \\ 2.153, & \text{Bipolar}. \end{cases}$$

Stagnation

Slightly beyond stability limit

Envelope model consistent with constants of the motion in linear field approximation describes beam focusing

rms envelope equation derived in usual manner by averaging over the particle equations of motion: $\Phi \equiv q\phi_0/\mathcal{E}_b$

$$R'' - \frac{1/2}{1-\Phi}\frac{\partial \Phi}{\partial z}R' - \frac{1/4}{1-\Phi}\frac{\partial^2 \Phi}{\partial z^2}R - \frac{1}{(1-\Phi)^{3/2}}\frac{Q}{R} - \frac{1}{1-\Phi}\frac{2\langle L_z\rangle_\perp^2/(m\mathcal{E}_b)}{R^3} - \frac{1}{1-\Phi}\frac{\varepsilon^2}{R^3} = 0$$

Here,

$R \equiv 2\sqrt{\langle x^2\rangle_\perp} = \sqrt{2\langle r^2\rangle_\perp}$ Statistical edge radius

$\varepsilon = \text{const}$ Usual rms edge Emittance before entering Einzel lens

$\langle L_z\rangle_\perp = \text{const}$ Beam angular momentum (zero most cases)

Matched envelope solution with the periodicity of lattice has optimal transport properties because it minimizes beam excursions

$$R(z + L_p) = R(z)$$

Example matched envelopes with strong space-charge

$r_p = 30$ mm $\quad qV/\mathcal{E}_b = 0.25 \quad Q = 5 \times 10^{-4}$

$\sigma_0 = 6.82°$ $\quad\quad$ $\sigma_0 = 12.46°$

$\sigma/\sigma_0 = 0.016$ $\quad\quad$ $\sigma/\sigma_0 = 0.0338$

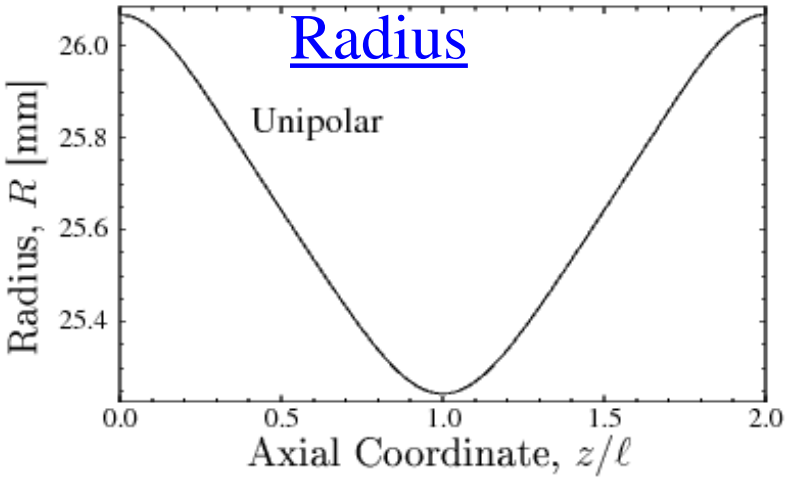

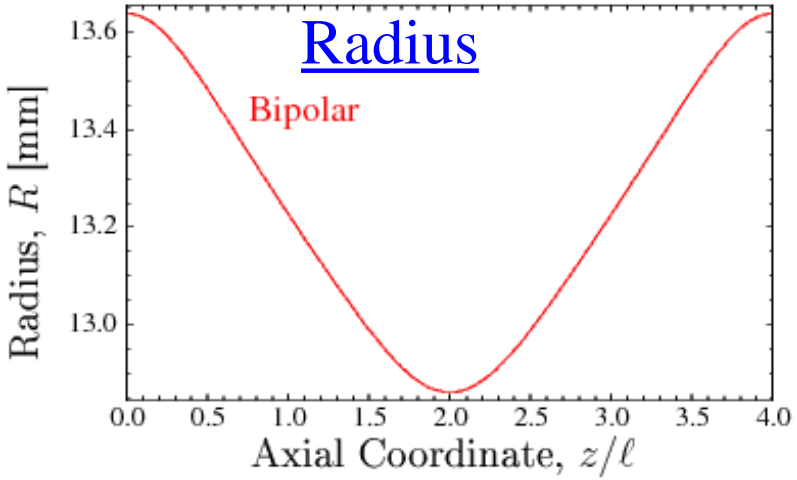

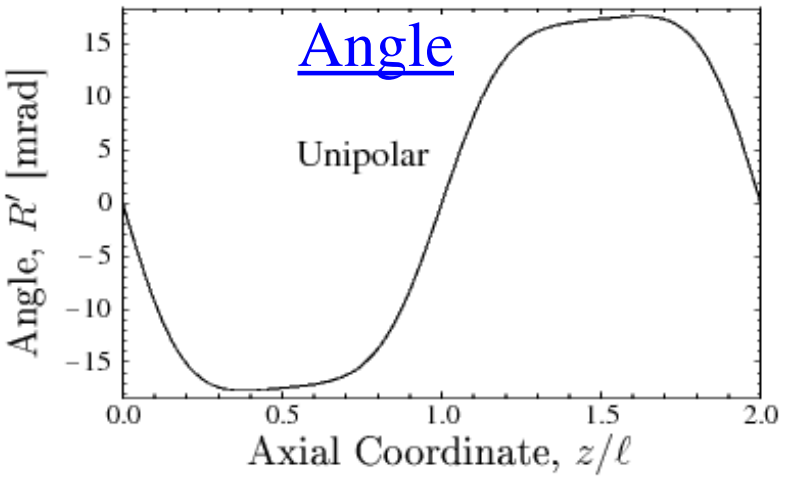

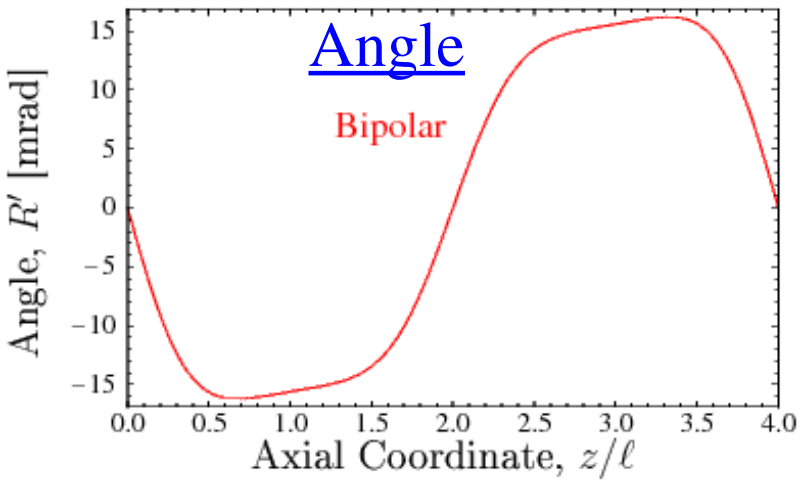

Note comparatively small envelope oscillations!

~ 1% unipolar $\quad\quad$ ~3% bipolar

Characteristic particle oscillations within the beam typically have extremely low phase advances

Bipolar Focusing with: $r_p = 30$ mm $\quad qV/\mathcal{E}_b = 0.5$ $\quad Q = 5 \times 10^{-4}$

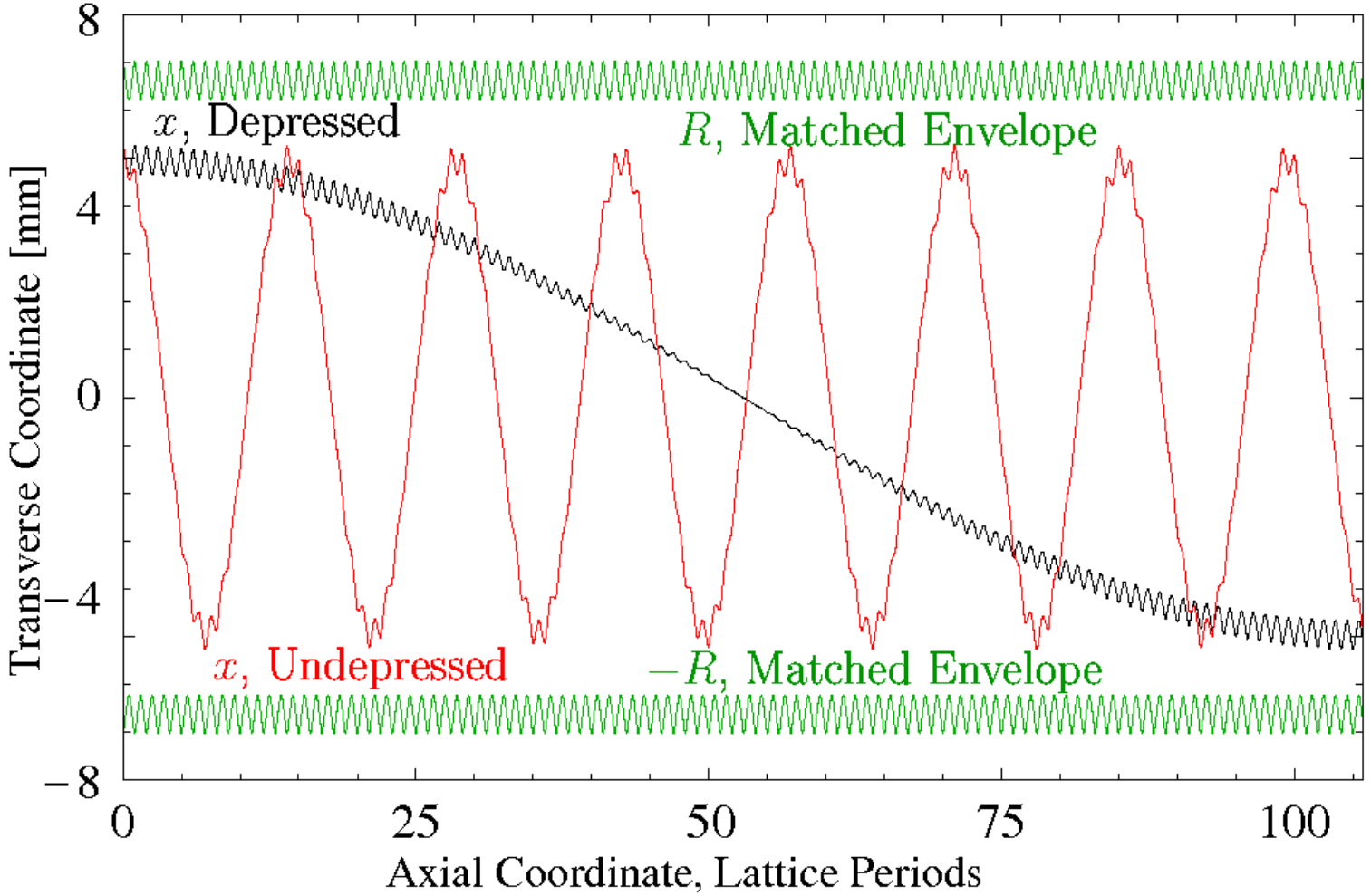

$\sigma_0 = 25.36°$

$\sigma = 1.702°$

$\sigma/\sigma_0 = 0.0671$

- Shown for large bias to increase oscillation rate: typical numbers much slower!
- Very low phase advances suggest a high degree of stability

Transformed envelope equations can simplify analysis analogously to the single-particle case

Take:

$$\tilde{R} \equiv 2\sqrt{\langle \tilde{x}^2 \rangle_\perp} = \sqrt{v_z} R \qquad \text{and} \qquad \mathcal{R} \equiv \tilde{R}/(2\mathcal{E}_b/m)^{1/4}$$

$$\Longrightarrow \quad R = \frac{1}{(1-\Phi)^{1/4}} \mathcal{R}$$

This gives:

$$\mathcal{R}'' + \kappa \mathcal{R} - \frac{1}{1-\Phi}\frac{Q}{\mathcal{R}} - \frac{2\langle L_z \rangle_\perp^2/(m\mathcal{E}_b)}{\mathcal{R}^3} - \frac{\varepsilon^2}{\mathcal{R}^3} = 0$$

$$\kappa(z) = \frac{3}{16}\left(\frac{\partial\Phi/\partial z}{1-\Phi}\right)^2 \qquad \Phi = \frac{q\phi_0}{\mathcal{E}_b}$$

Matched solution is periodic in transformed or untransformed variables:

$$R(z + L_p) = R(z)$$

$$\Longrightarrow \quad \mathcal{R}(z + L_p) = \mathcal{R}(z)$$

Previously shown matched envelopes both without space-charge and with strong space-charge show little oscillation when expressed in transformed variables

Transformed Matched Envelope Radius

Unipolar, $Q = 0$

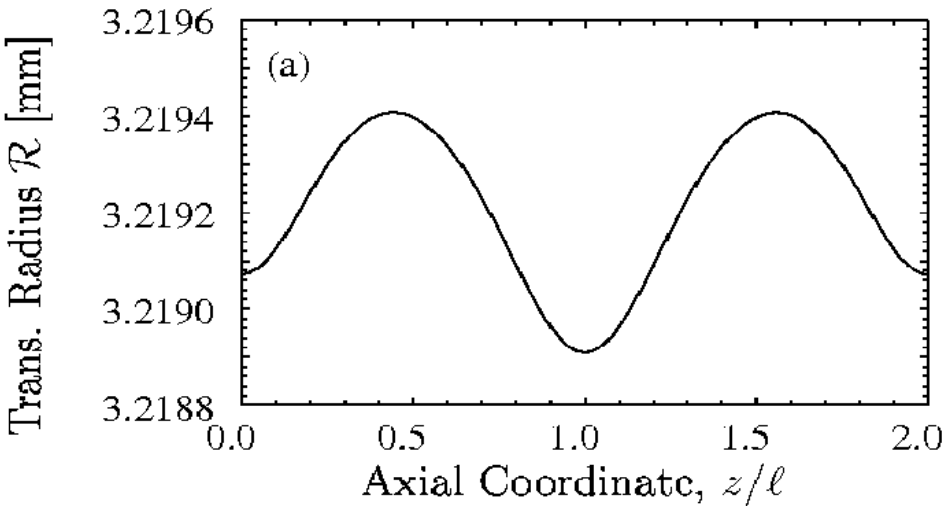

Unipolar, $Q = 5 \times 10^{-4}$

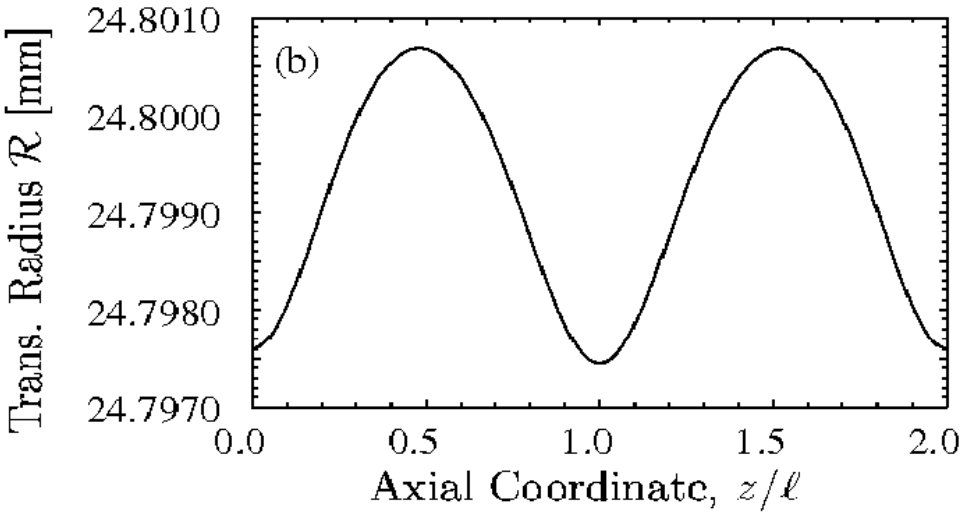

Note scale: Matched envelope variations ~ 0.01% average value!

Accurate transport scaling relations derived which can be used to rapidly evaluate Einzel lens focusing

Use near constancy of transformed matched envelope and simpler analog of quadrupole matched envelope analysis by Ed Lee (Phys. Plasmas 2002) to derive approx formulas for matched envelope properties:

Transformed average matched envelope:

$$\overline{\kappa \mathcal{R}} - \overline{\frac{1}{1-\Phi}} \frac{Q}{\overline{\mathcal{R}}} - \frac{2\langle L_z \rangle_\perp^2 / (m\mathcal{E}_b) + \varepsilon^2}{\overline{\mathcal{R}}^3} \simeq 0$$

Average untransformed radius:

$$\overline{R} \simeq \overline{\frac{1}{(1-\Phi)^{1/4}}} \overline{\mathcal{R}}$$

$$\kappa(z) = \frac{3}{16} \left(\frac{\partial \Phi / \partial z}{1-\Phi} \right)^2$$

$$\Phi = \frac{q\phi_0}{\mathcal{E}_b}$$

Max envelope excursion:

$$\mathrm{Max}[R] \simeq \frac{1}{(1-\mathrm{Max}[\Phi])^{1/4}} \overline{\mathcal{R}}$$

Numerical checks indicate formulas accurate to ~ 0.01 % for a wide range of system parameters!

For a limited range of bias the transportable perveance for optimized geometry is accurately estimated by a very simple formula:

$$Q \leq 0.0100 n_s^2 \left(\frac{qV}{\mathcal{E}_b}\right)^2 \left(\frac{\mathrm{Max}[R]}{r_p}\right)^2$$

$$n_s \equiv \frac{L_p}{2\ell} = \begin{cases} 1, & \text{Unipolar,} \\ 2, & \text{Bipolar,} \end{cases}$$

$$\frac{r_p}{L_p} = 0.2342 \qquad \frac{qV}{\mathcal{E}_b} \lesssim 0.5$$

- Bipolar transports 4x unipolar for same $qV/\mathcal{E}_b$
  - Bipolar and unipolar equally efficient in terms of peak to peak voltage

Scaling relations give transportable Q for a space-charge dominated beam with optimal geometry for unipolar and bipolar systems

Transportable perveance depends only on filling factor and scaled bias:

$$\frac{\mathrm{Max}[R]}{r_p} = \text{Beam Extent in Aperture (Filling Factor)} \qquad \frac{qV}{\mathcal{E}_b} = \text{Scaled Bias (Bias over Beam Energy)}$$

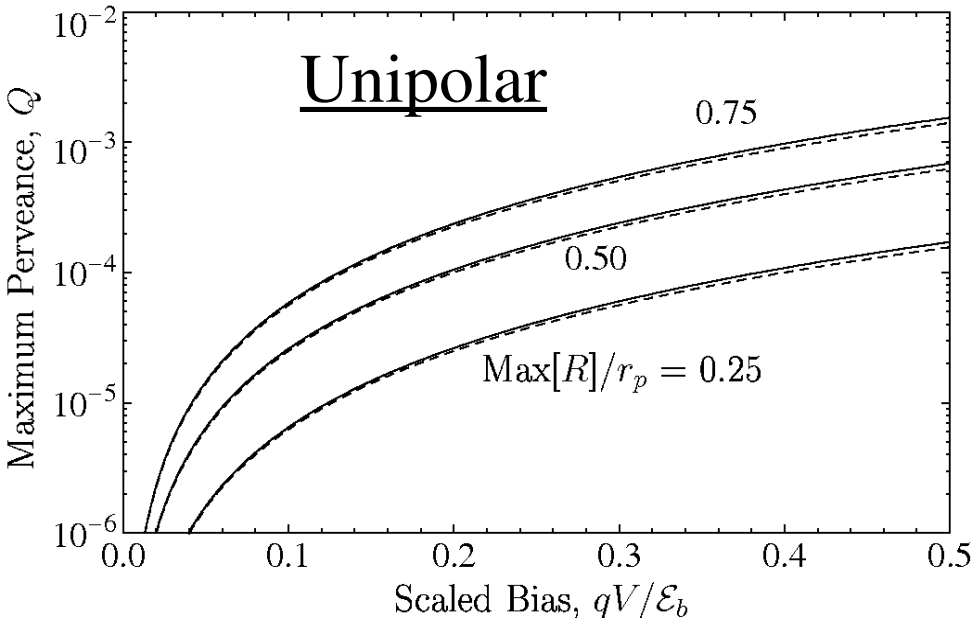

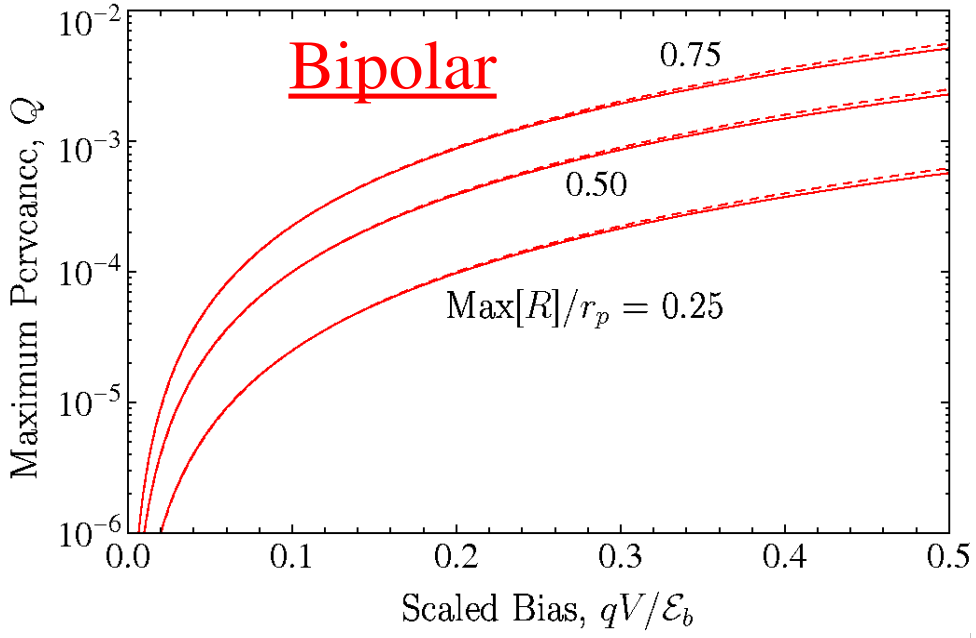

- Dashed curves based on more approximate, scaling equation

Full Warp *r-z* PIC beam simulations applied to verify good transport over many lattice periods

Simulations explore:

- Viability of transport due to nonlinear fields
  - Long path length to sensitively probe possible emittance growth
- Matching and beam control

Simulation setup:

- High resolution/statistics enabled by *r-z* simulations
- Washer structures placed on grid with detailed particle scraping
- One lattice period of matched initial beam formed
  - Various (Semi-Gauss, Waterbag, Thermal) distributions injected on left on a stationary grid with particle absorbing boundary conditions on right
  - z-velocity spread ½ transverse spread to suppress $\perp$ / $\parallel$ unstable modes
  - Advanced to fill period with stationary beam
  - Injection conditions iterated to "nonlinearly" match envelope
  - Simulation changed to moving grid with periodic particle boundary conditions and advanced
- Period average envelope and normalized emittance histories analyzed
  - Allows low noise resolution of mismatch and emittance growth

High space-charge intensity and aperture fill factor transport result in negligible mismatch and emittance growth in spite of large applied field nonlinearities

Parameters: $Q = 4 \times 10^{-4}$, $\varepsilon = 50$ mm-mrad initial waterbag distribution
$r_p = 40$ mm

Envelope

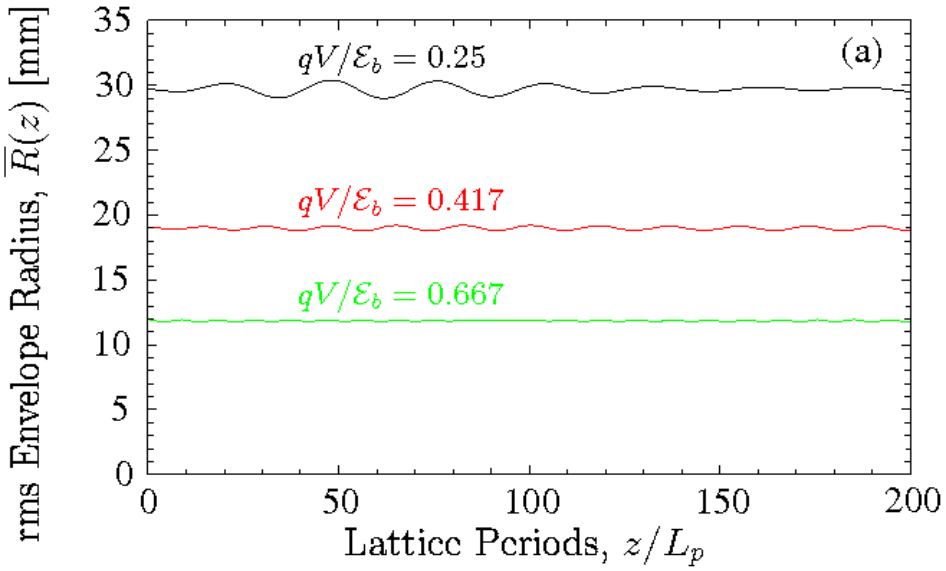

Emittance Evolution

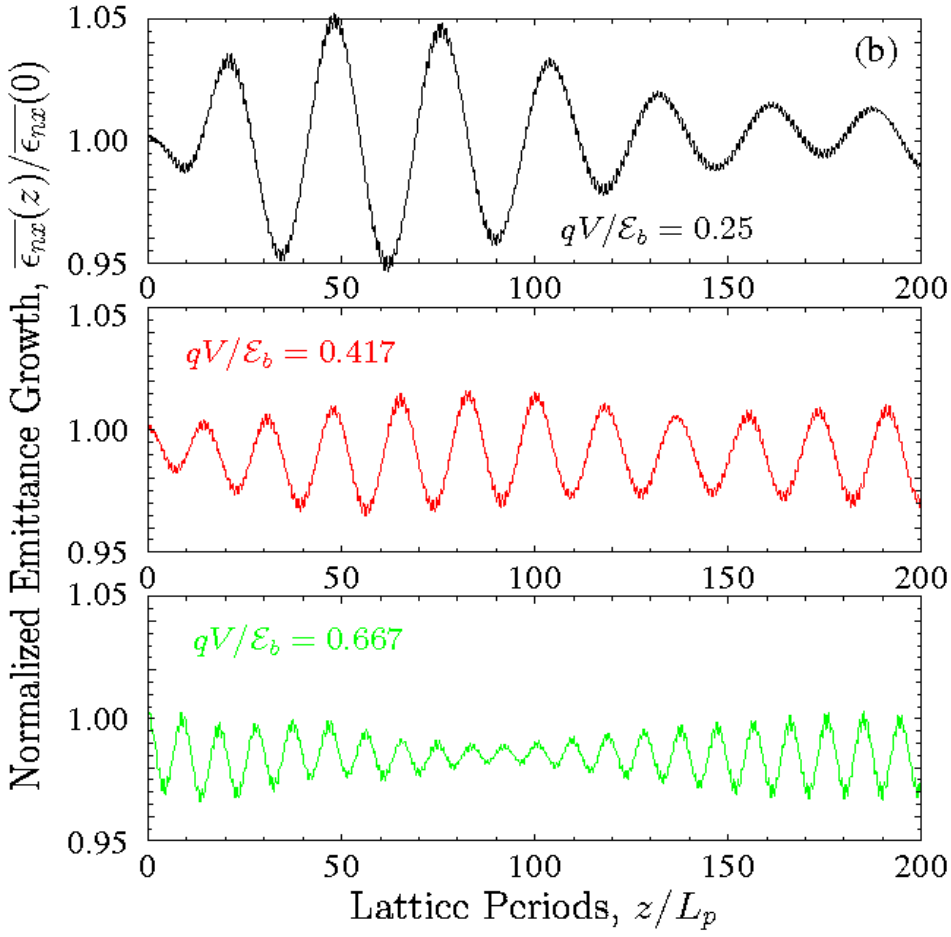

- Results similarly good for initial semi-Gaussian and thermal distributions
- Emittance evolutions less for more strongly focused beams

At high aperture fill factor the density becomes nonuniform with distorted phase-space due to nonlinear focusing

Initial Density/Phase-Space

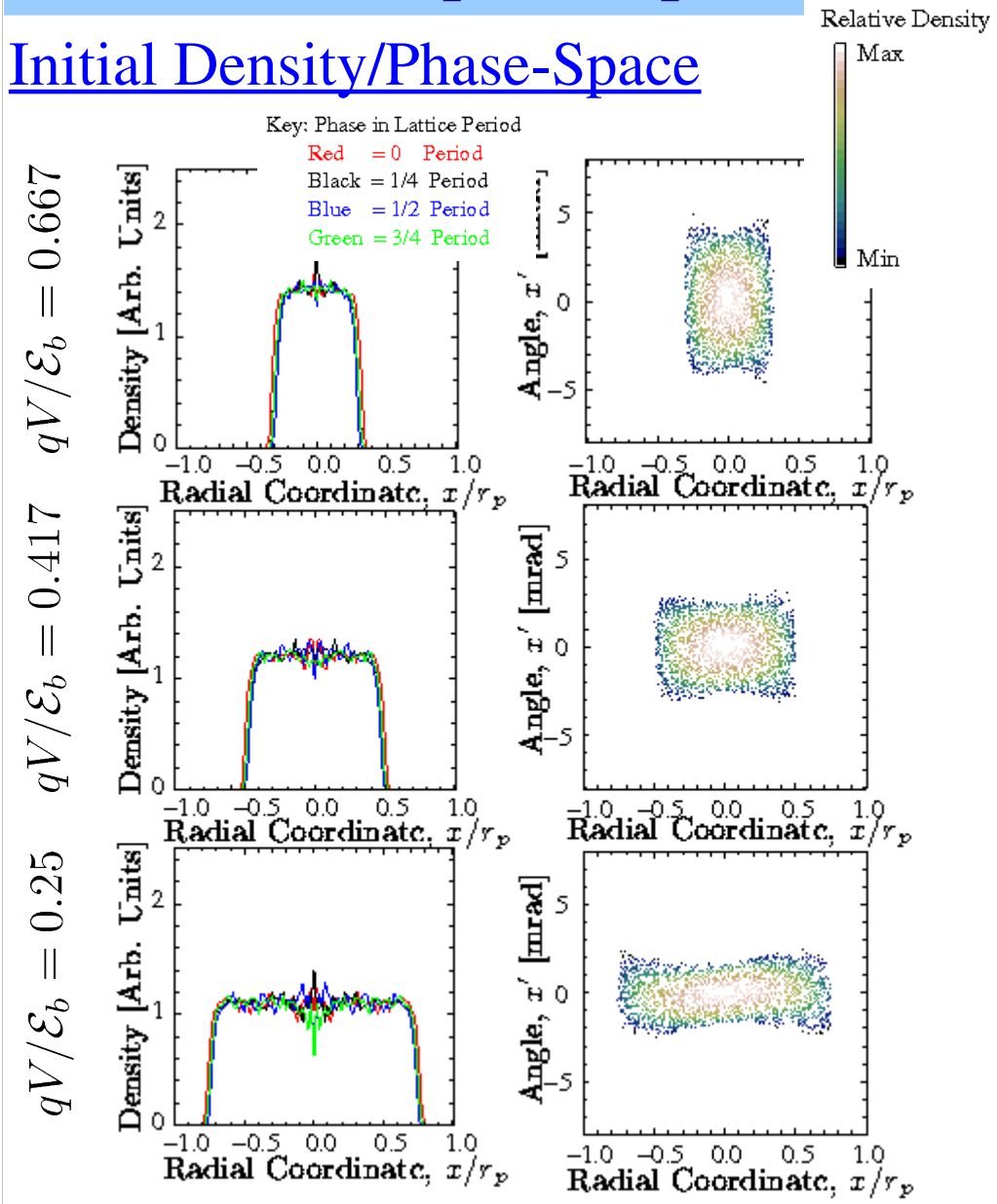

At 100 periods

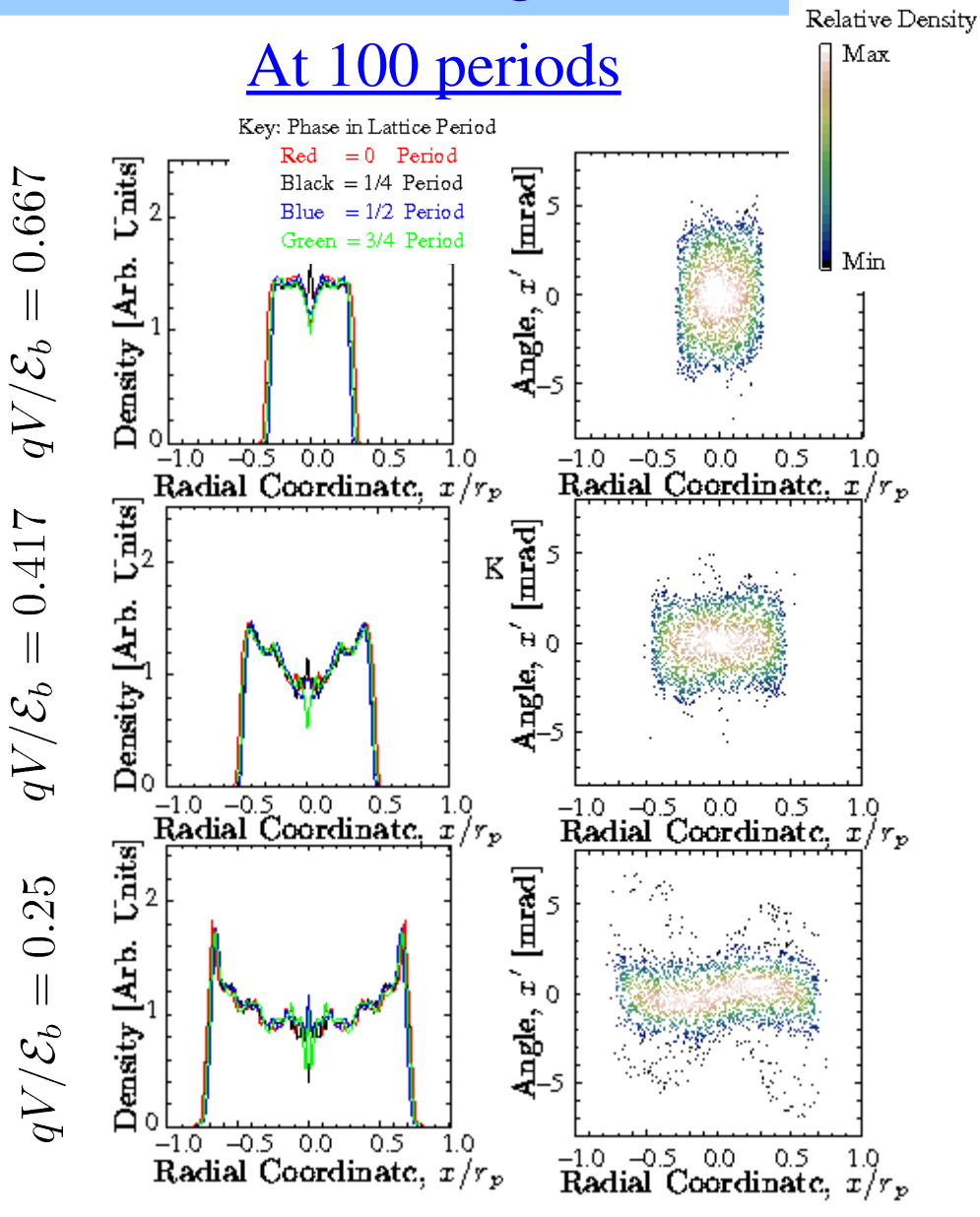

Summary

- Optimization of "stacked-washer" Einzel lens systems carried out:
  - Simple, accurate linear applied field model derived
  - Needed washer radial extents, radiusing for breakdown suppression, and applied field nonlinearities quantified
  - Linear particle/envelope model derived and focusing geometry optimized
  - Simple transport scaling derived shows high perveance transport possible
- Warp PIC simulations verify that high fill factor and high perveance transport preserves beam quality
  - No emittance growth over long transport in spite of high nonlinear fields
- Technology attractive for plethora of near-injector applications
  - Simple and economical
  - Optimization clarifies range of max voltage/focusing can work
  - No magnetic field to penetrate source (emittance penalty)

Extensive article detailing work now mostly completed for submission to PRSTAB

Selected Topics on Space-Charge Effects in Intense Beams

1) US Particle Accelerator School and UC Berkeley courses on "Beam Physics with Intense Space-Charge"

2) Theory and numerical simulations on optimal Einzel lens transport

3) Multipole expansion for realistic modeling of focusing optics

4) Space-Charge induced transport limits in quadrupole focusing channels

5) Nonlinear focusing channel for stable beam transport and possible application to NGLS/APEX

Background/Motivation

Need reliable and fully general 3D description of field from magnets for high level computer simulations

- Field terms associated with:
  - Field Errors: Transverse multipole fields from non-ideal windings
  - Misalignments: Coordinate system not on center (offset + tilt)
- Descriptions of fields should be compact and general for ease of use and reduce to intuitive "standard" forms to aid physics interpretation

Approaches:

1) Direct: Measure 3D field components on grid and import in code
- Very large amount of field data renders impractical
- No information on relationship of design fields relative to error terms

2) Multipole: Use 3D Multipole field expansions
- Already in Warp code and debugged
- Can efficiently extract multipole terms from (minimal) measured field data on surfaces

General 3D Multipole Expansion: Lund HIF Note 96-10, 1996

Field solutions to the homogenous Maxwell equations:

$$\nabla \cdot \mathbf{B} = 0 \qquad\qquad \nabla \times \mathbf{B} = 0$$

can be expanded within a cylindrical vacuum region $r < r_p$ (Aperture) as:

$$B_r = -\sum_{\nu=0}^{\infty} \frac{1}{2(\nu+1)} \frac{db_{0,\nu}(z)}{dz} r^{2\nu+1}$$
$$+ \sum_{n=1}^{\infty}\sum_{\nu=0}^{\infty} b_{n,\nu}(z) \left[1 + \frac{2\nu}{n}\right] r^{n-1+2\nu} \cos[n\theta + \psi_n(z)],$$

$$B_\theta = -\sum_{n=1}^{\infty}\sum_{\nu=0}^{\infty} b_{n,\nu}(z) r^{n-1+2\nu} \sin[n\theta + \psi_n(z)],$$

$$B_z = \sum_{\nu=0}^{\infty} b_{0,\nu}(z) r^{2\nu} + \sum_{n=1}^{\infty}\sum_{\nu=0}^{\infty} \frac{1}{n} \frac{db_{n,\nu}(z)}{dz} r^{n+2\nu} \cos[n\theta + \psi_n(z)]$$
$$- \sum_{n=1}^{\infty}\sum_{\nu=0}^{\infty} \frac{1}{n} \frac{d\psi_n(z)}{dz} b_{n,\nu}(z) r^{n+2\nu} \sin[n\theta + \psi_n(z)],$$

$$B_r = \cdots, \qquad B_\theta = -\sum_{n=1}^{\infty}\sum_{\nu=0}^{\infty} b_{n,\nu}(z) r^{n-1+2\nu} \sin[n\theta + \psi_n(z)], \qquad B_z = \cdots$$

$n = 0, 1, 2, 3, \cdots$ Azimuthal Harmonic Number

$\nu = 0, 1, 2, 3, \cdots$ Radial Index ... necessary in 3D ....

$b_{n,\nu}(z)$ Multipole Amplitude Function (positive or negative)

$\psi_n(z)$ Multipole Phase Function

Due to transverse symmetries:

- $\nu = 0$ amplitude functions are called fundamental amplitudes
- $\nu > 0$ amplitude functions are called pseudomultipole amplitudes

Pseudomultipole amplitudes are related to fundamental amplitudes and phase functions by:

$$b_{n,\nu}(z)\cos\psi_n(z) = \frac{(-1)^\nu n!}{4^\nu \nu!(n+\nu)!}\frac{d^{2\nu}}{dz^{2\nu}}\{b_{n,0}(z)\cos\psi_n(z)\}$$

$$b_{n,\nu}(z)\sin\psi_n(z) = \frac{(-1)^\nu n!}{4^\nu \nu!(n+\nu)!}\frac{d^{2\nu}}{dz^{2\nu}}\{b_{n,0}(z)\sin\psi_n(z)\}$$

- Set of fundamental amplitudes and phases $\{b_{n,0}(z), \psi_n(z)\}$ specify field

Simplification for systems with axially invariant transverse symmetry

Systems with transverse symmetries which do not vary in *z* have:

$$\psi_n(z) = \text{const}$$

In this case the multipole expansions reduce to the simpler form:

$$B_r = -\sum_{\nu=0}^{\infty} \frac{1}{2(\nu+1)} \frac{db_{0,\nu}(z)}{dz} r^{2\nu+1}$$
$$+ \sum_{n=1}^{\infty}\sum_{\nu=0}^{\infty} b_{n,\nu}(z) \left[1 + \frac{2\nu}{n}\right] r^{n-1+2\nu} \cos[n\theta + \psi_n],$$

$$B_\theta = -\sum_{n=1}^{\infty}\sum_{\nu=0}^{\infty} b_{n,\nu}(z) r^{n-1+2\nu} \sin[n\theta + \psi_n],$$

$$B_z = \sum_{\nu=0}^{\infty} b_{0,\nu}(z) r^{2\nu} + \sum_{n=1}^{\infty}\sum_{\nu=0}^{\infty} \frac{1}{n} \frac{db_{n,\nu}(z)}{dz} r^{n+2\nu} \cos[n\theta + \psi_n],$$

$$b_{n,\nu}(z) = \frac{(-1)^\nu n!}{4^\nu \nu!(n+\nu)!} \frac{d^{2\nu}}{dz^{2\nu}} b_{n,0}(z)$$

For harmonic number $n \geq 1$ and radial index ν, the transverse field components produced vary as

Radial: $B_\perp \sim b_{n,\nu}(z) r^{n-1+2\nu}$

Azimuthal: $B_\perp \sim b_{n,\nu}(z) \cos[n\theta + \psi_n(z)]$

A special case, for an ideal solenoid, the expansion can be further reduced to the familiar form:

$$B_r = -\sum_{\nu=0}^{\infty} \frac{(-1)^\nu}{\nu!(\nu+1)!} \frac{\partial^{2\nu+1}}{\partial z^{2\nu+1}} B_{z0}(z) \left(\frac{r}{2}\right)^{2\nu+1} = -\frac{1}{2}\frac{dB_{z0}(z)}{dz} r + \cdots$$

$$B_z = \sum_{\nu=0}^{\infty} \frac{(-1)^\nu}{(\nu!)^2} \frac{\partial^{2\nu}}{\partial z^{2\nu}} B_{z0}(z) \left(\frac{r}{2}\right)^{2\nu} = B_{z0}(z) + \cdots$$

Linear Terms

NonLinear Terms

$$B_{z0}(z) \equiv B_z(r=0,z) = b_{0,0}(z)$$

$$\psi_0 \equiv 0$$

- $n = 0$, $\nu = 0, 1, 2, \cdots$ terms describe an ideal, axisymmetric solenoid

Axially averaged multipole functions and relation to 2D transverse multipole expansions

Define an axial average:

$$\overline{\cdots} \equiv \frac{1}{\ell}\int_{-\infty}^{\infty} dz \ \cdots$$

- ℓ aritrary, but usually set to effective field length of magnet

Average of 3D expansion gives:

$$\overline{B_r} = \sum_{n=1}^{\infty} \overline{b_{n,0}\cos[n\theta+\psi_n]} r^{n-1} \quad \Longrightarrow \quad \overline{B_r} = \sum_{n=1}^{\infty} \overline{b_{n,0}}\cos[n\theta+\overline{\psi_n}] r^{n-1}$$

$$\overline{B_\theta} = -\sum_{n=1}^{\infty} \overline{b_{n,0}\sin[n\theta+\psi_n]} r^{n-1} \quad \overline{B_\theta} = -\sum_{n=1}^{\infty} \overline{b_{n,0}}\sin[n\theta+\overline{\psi_n}] r^{n-1}$$

$$\overline{B_z} = \overline{b_{0,0}}$$

- Reduction of transverse components always carried out by defining and effective amplitude and phase
  - Exactly as expressed for axially invariant transverse symmetry

Transverse averaged field components are the 2D fields:

- Satisfy 2D transverse Maxwell Equations

$$\frac{\partial \overline{B_x}(x,y)}{\partial x} = -\frac{\partial \overline{B_y}(x,y)}{\partial y} \qquad \frac{\partial \overline{B_x}(x,y)}{\partial y} = \frac{\partial \overline{B_y}(x,y)}{\partial x}$$

These are the Cauchy-Riemann conditions for a complex field

$$\underline{B}^* \equiv \overline{B_x} - i\overline{B_y} \qquad i \equiv \sqrt{-1}$$

to be an anlytical function of the complex coordinate

$$\underline{z} \equiv x + iy$$

Thus the complex field is expandable in a Laurent series as

$$\underline{B}^* = \overline{B_x} - i\overline{B_y} = \sum_{n=1}^{\infty} \underline{b}_n \underline{z}^{n-1}$$

and the 2D complex multipole coefficients $\underline{b}_n$ can be identified in terms of the 3D multipole functions as:

$$\underline{b}_n = \overline{b_{n,0}} e^{i\overline{\psi_n}}$$

The complex 2D multipole coefficients are typically expanded as

$$\underline{b}_n = \mathcal{A}_n - i\mathcal{B}_n$$

$\mathcal{B}_n$ = Normal multipole component

$\mathcal{A}_n$ = Skew multipole component

Field components produced have projections

Cartesian projections: $\overline{B_x} - i\overline{B_y} = (\mathcal{A}_n - i\mathcal{B}_n)(x+iy)^{n-1}$

Index	Name	Normal ($\mathcal{A}_n = 0$)		Skew ($\mathcal{B}_n = 0$)	
n		$\overline{B_x}/\mathcal{B}_n$	$\overline{B_y}/\mathcal{B}_n$	$\overline{B_x}/\mathcal{A}_n$	$\overline{B_y}/\mathcal{A}_n$
1	Dipole	0	1	1	0
2	Quadrupole	y	x	x	$-y$
3	Sextupole	$2xy$	$x^2 - y^2$	$x^2 - y^2$	$-2xy$
4	Octupole	$3x^2y - y^3$	$x^3 - 3xy^2$	$x^3 - 3xy^2$	$-3x^2y + y^3$
5	Decapole	$4x^3y - 4xy^3$	$x^4 - 6x^2y^2 + y^4$	$x^4 - 6x^2y^2 + y^4$	$-4x^3y + 4xy^3$

Cylindrical projections: $\overline{B_r} - i\overline{B_\theta} = (\mathcal{A}_n - i\mathcal{B}_n)r^{n-1}e^{in\theta}$

Index	Name	Normal ($\mathcal{A}_n = 0$)		Skew ($\mathcal{B}_n = 0$)	
n		$\overline{B_r}/\mathcal{B}_n$	$\overline{B_\theta}/\mathcal{B}_n$	$\overline{B_r}/\mathcal{A}_n$	$\overline{B_\theta}/\mathcal{A}_n$
1	Dipole	$\sin(\theta)$	$\cos(\theta)$	$\cos(\theta)$	$-\sin(\theta)$
2	Quadrupole	$r\sin(2\theta)$	$r\cos(2\theta)$	$r\cos(2\theta)$	$-r\sin(2\theta)$
3	Sextupole	$r^2\sin(3\theta)$	$r^2\cos(3\theta)$	$r^2\cos(3\theta)$	$-r^2\sin(3\theta)$
4	Octupole	$r^3\sin(4\theta)$	$r^3\cos(4\theta)$	$r^3\cos(4\theta)$	$-r^3\sin(4\theta)$
5	Decapole	$r^4\sin(5\theta)$	$r^4\cos(5\theta)$	$r^4\cos(5\theta)$	$-r^4\sin(5\theta)$

Calculation of 3D Multipole Coefficients From Measured Field Data

Follow Venturini and Dragt, Nuc. Inst. Meth. A **387-392**, 427 (1999) and calculate the scalar potential on a cylindrical surface and relate to field measurements on the surface to identify the 3D multipole functions

- Intuitive: electrostatic equivalent problem set by boundary data in a source free region
- Procedure formulated not use derivatives of field data
  - Integration (Fourier Series and Transforms) employed which should smooth noisy data
- General while promising good accuracy
  - Field errors sampled on larger radial surface easier to resolve
- Big savings in measurement data: Example NDCX-II Solenoids

$$\text{Data Points}_{3D} = \underbrace{3}_{\text{Field}} \times \underbrace{\frac{(\ell + 6r_i)}{dz}}_{\text{z-dir}} \times \underbrace{\left(2\frac{r_p}{dx}\right)^2}_{\text{perp-dir}} \sim 1.2 \text{ Million}$$

$$\text{Data Points}_{\text{surface}} = 1 \times \frac{(\ell + 6r_o)}{dz} \times (4n_{\max}) \sim 10.4 \text{ k}$$

Factor 115 Reduction!

$$dz = dx = 2 \text{ mm} \quad n_{\max} = 10$$

Scalar Magnetic Potential:

$$\mathbf{B} = -\nabla\phi = -\hat{\mathbf{r}}\frac{\partial}{\partial r}\phi - \hat{\theta}\frac{1}{r}\frac{\partial}{\partial\theta}\phi - \hat{\mathbf{z}}\frac{\partial}{\partial z}\phi$$

$$\phi = -\sum_{\nu=0}^{\infty} r^{2\nu} \int_{-\infty}^{z} d\tilde{z}\; b_{0,\nu}(\tilde{z})$$

$$- \sum_{n=1}^{\infty}\sum_{\nu=0}^{\infty} \frac{1}{n} b_{n,\nu}(z) r^{n+2\nu} \cos[n\theta + \psi_n(z)] \;+\; \text{const}$$

Expand Transverse 3D Field Components:

Fourier series of periodic azimuthal dependance on a surface at $r = R$

$$B_r(R,\theta,z) = \sum_{n=0}^{\infty} \left[B^c_{r,n}(R,z)\cos(n\theta) + B^s_{r,n}(R,z)\sin(n\theta)\right]$$

$$B_\theta(R,\theta,z) = \sum_{n=1}^{\infty} \left[B^c_{\theta,n}(R,z)\cos(n\theta) + B^s_{\theta,n}(R,z)\sin(n\theta)\right]$$

$B^c_{r,n}(R,z)$ = Fourier Coefficient
harmonic n, cosine-like function

Radial Field Measurements on Surface:

- Give *all* harmonic components
  - Solenoidal amplitudes and
    transverse multipole amplitudes and phases

n = 0 terms

$$b_{0,\nu}(z) = \frac{i}{4^\nu(\nu!)^2}\int_{-\infty}^{\infty}\frac{dk}{\sqrt{2\pi}}\frac{k^{2\nu}}{I_0'(kR)}e^{ikz}\int_{-\infty}^{\infty}\frac{d\tilde{z}}{\sqrt{2\pi}}e^{-ik\tilde{z}}B^c_{r,n}(R,\tilde{z})$$

$n > 0$ terms

$$b_{n,\nu}(z)e^{i\psi_n(z)} = \frac{n}{2^{n+2\nu}\nu!(n+\nu)!}\int_{-\infty}^{\infty}\frac{dk}{\sqrt{2\pi}}\frac{k^{n-1+2\nu}}{I_n'(kR)}e^{ikz} \times\int_{-\infty}^{\infty}\frac{d\tilde{z}}{\sqrt{2\pi}}e^{-ik\tilde{z}}\left[B^c_{r,n}(R,\tilde{z}) - iB^s_{r,n}(R,\tilde{z})\right]$$

$I_n(x)$ = Modified Bessel Function, 1st Kind, order n

Azimuthal Field Measurements:

- Give *only* transverse multipole amplitudes and phases
  - Redundant data for azimuthal field can be used for consistency/accuracy checks

n > 0 terms

$$b_{n,\nu}(z)e^{i\psi_n(z)} = -\frac{R}{2^{n+2\nu}\nu!(n+\nu)!}\int_{-\infty}^{\infty}\frac{dk}{\sqrt{2\pi}}\frac{k^{n+2\nu}}{I_n(kR)}e^{ikz} \times \int_{-\infty}^{\infty}\frac{d\tilde{z}}{\sqrt{2\pi}}e^{-ik\tilde{z}}\left[B^s_{\theta,n}(R,\tilde{z}) + iB^c_{\theta,n}(R,\tilde{z})\right]$$

$I_n(x) =$ Modified Bessel Function, 1st Kind, order n

Axial Field Measurements on-axis:

- Gives information on *n* = 0 solenoidal field components only
  - More accurate due to structure of formulas for *n* = 0

n = 0 terms

$$b_{0,0}(z) = B_{z0}(z) = B_z(r=0,z)$$

$$b_{0,\nu}(z) = \frac{1}{4^\nu(\nu!)^2}\int_{-\infty}^{\infty}\frac{dk}{\sqrt{2\pi}}k^{2\nu}e^{ikz}\int_{-\infty}^{\infty}\frac{d\tilde{z}}{\sqrt{2\pi}}e^{-ik\tilde{z}}B_{z0}(\tilde{z})$$

Summary

- A general 3D multipole expansion has been developed
  - Applicable to all magnet types: solenoid, dipole, quadrupole, ...
  - Implemented/benchmarked in the WARP code for realistic modeling
  - Symmetries of errors clarified by expansion terms aid physics interpretation
- Formulas derived to efficiently and accurately extract multipole expansion terms from measured field data on surfaces
  - Surface measurements of radial field rather than volumetric measurements of 3 field components for big reductions of measurements for realistic fields
  - Promises better accuracy: relevant errors larger to resolve on outer surface
- Applicable to NGLS/APEX for realistic modeling
  - Including centroid/alignment errors of solenoid inducing corkscrew modes which may reduce effective beam quality
  - Lab notes available fully detail formulation

Selected Topics on Space-Charge Effects in Intense Beams

1) US Particle Accelerator School and UC Berkeley courses on "Beam Physics with Intense Space-Charge"

2) Theory and numerical simulations on optimal Einzel lens transport

3) Multipole expansion for realistic modeling of focusing optics

4) Space-Charge induced transport limits in quadrupole focusing channels

5) Nonlinear focusing channel for stable beam transport and possible application to NGLS/APEX

Review: SBTE experiment at LBNL on quadrupole transport limits Higher order Vlasov instability with strong emittance growth/particle losses observed in broad parametric region below envelope band

[FODO Lattice; M.G. Tiefenback, Ph.D Thesis, UC Berkeley (1986)]

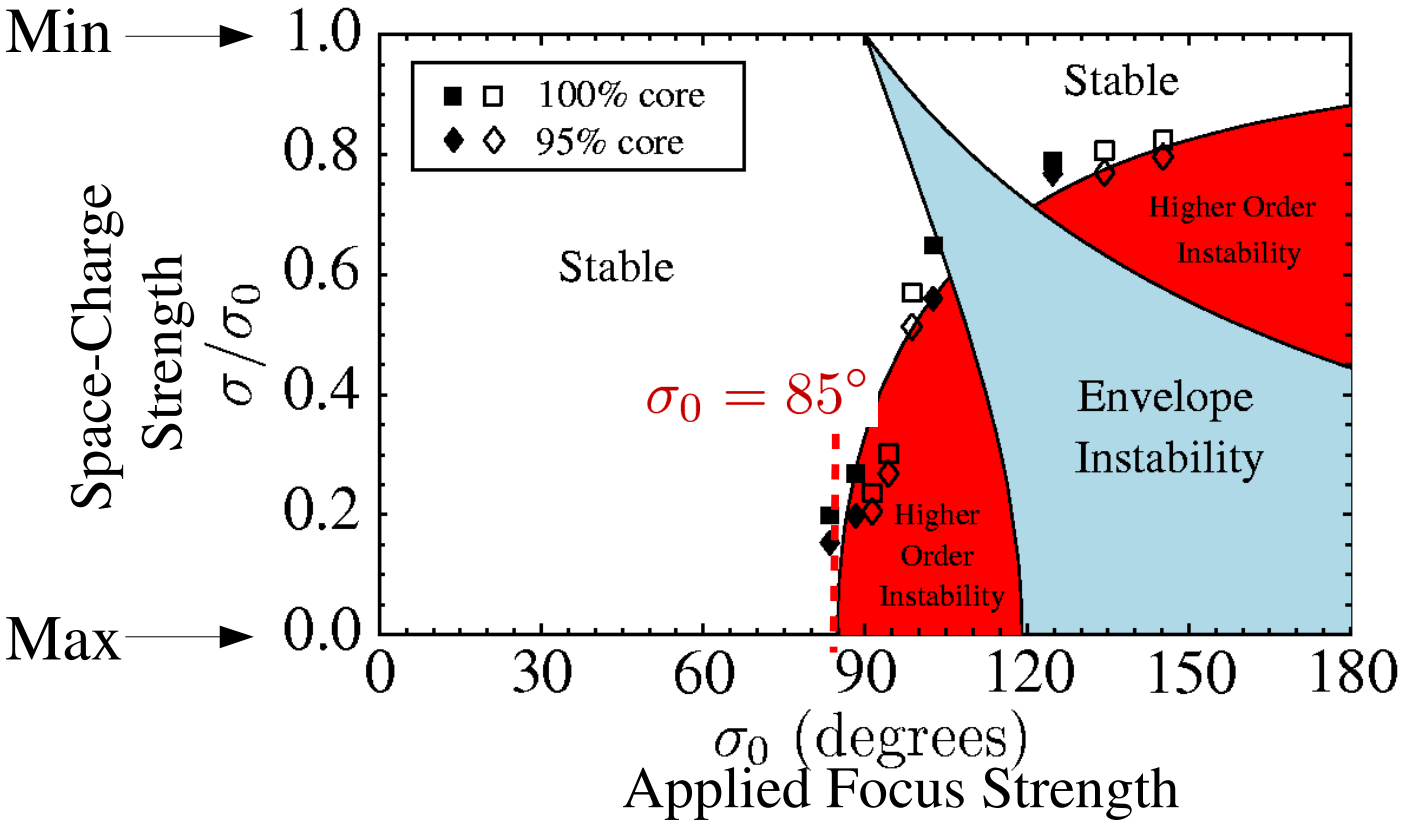

Evelope Instability Review:
Lund Bukh, PRSTAB 2004

Results summarized by $\sigma_0 \lesssim 85°$ for strong space-charge

- Reliably applied design criterion in the lab
- Limited theory understanding for 20+ years; Haber, Laslett simulations supported

Theory and simulation publications over-viewed here explain mechanism

Lund. Chawla, NIMA 2006 Lund, Barnard, Bukh, Chawla, Chilton, NIMA 2007

Parametric Warp PIC simulations of smooth, initially matched distributions have little emittance evolution outside of instability regions experimentally observed

Example: initial thermal equilibrium distribution:

Lund, Kikuchi, Davidson

PRSTAB 2009

- Density along *x*- and *y*-axes for 5 periods
- Emittance growth very small -- 5 period initial transient shown

Superimposed Density Snapshots

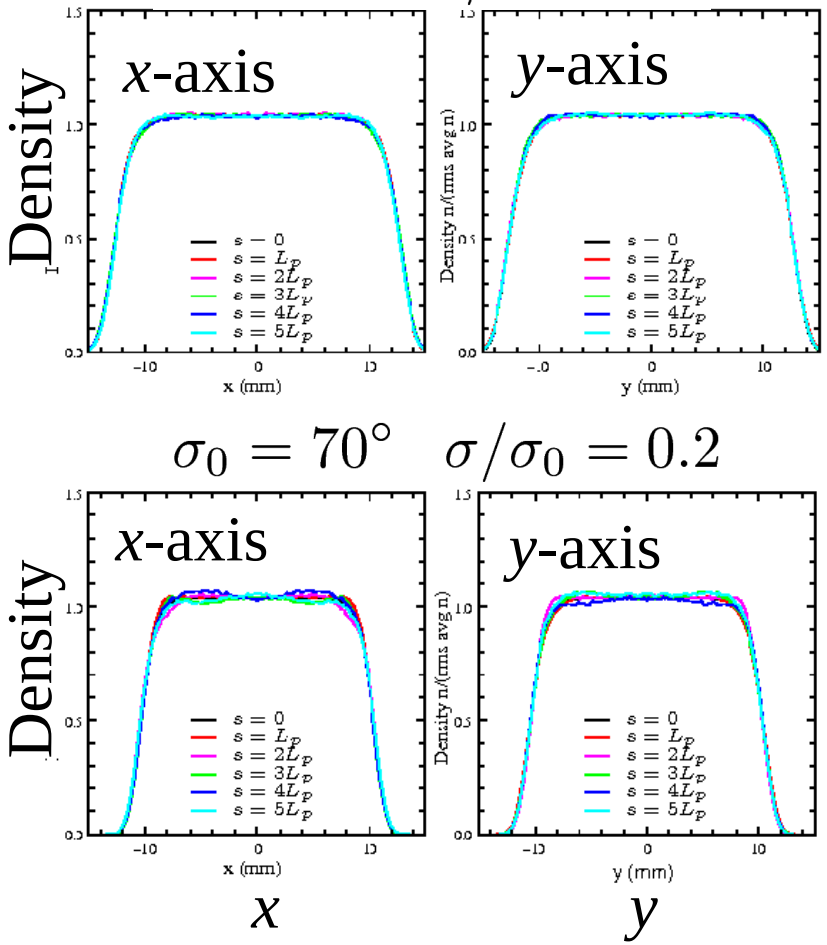

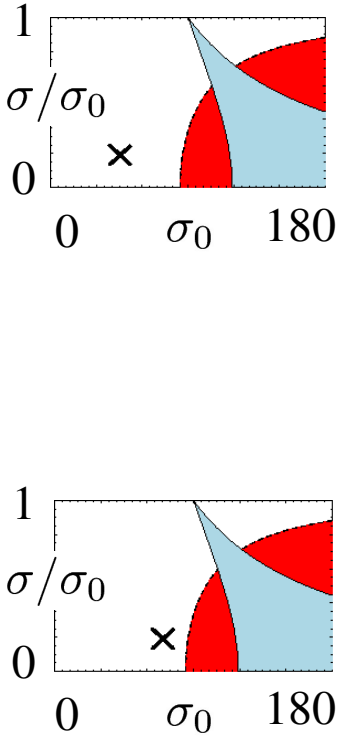

Emittance Evolution

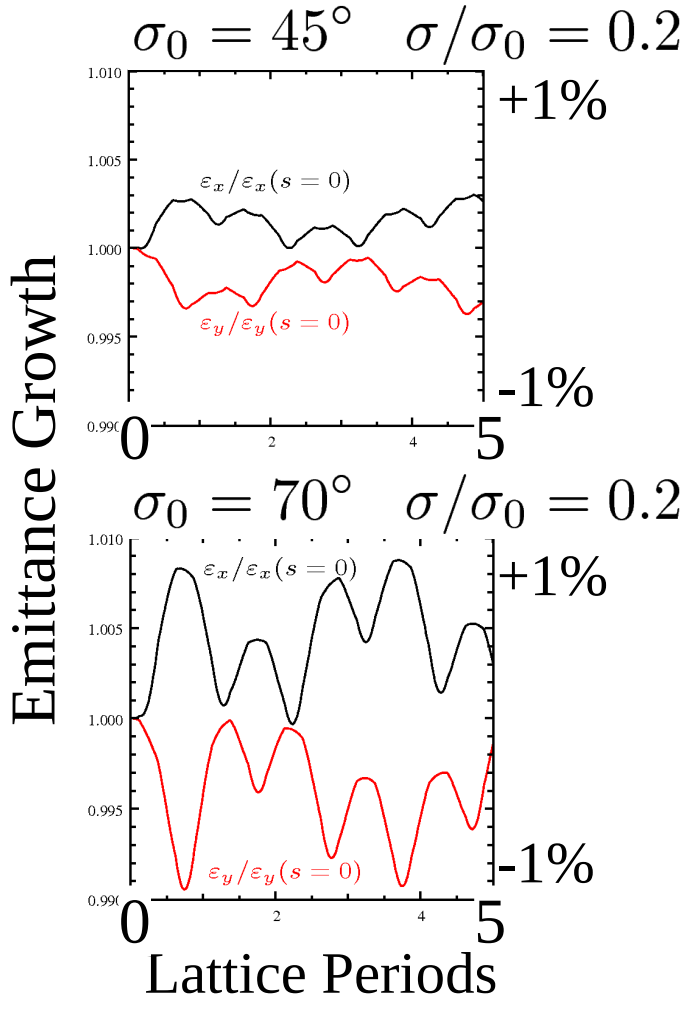

Warp simulations find broad instability region to the left of the envelope band -- features relatively insensitive to the form of the (non-singular) matched initial distribution

- Where unstable, growth becomes larger and faster with increasing σ_0

Example Parameters: $\sigma_0 = 110°$, $\sigma/\sigma_0 = 0.2$ ($L_p = 0.5$ m, $\eta = 0.5$)

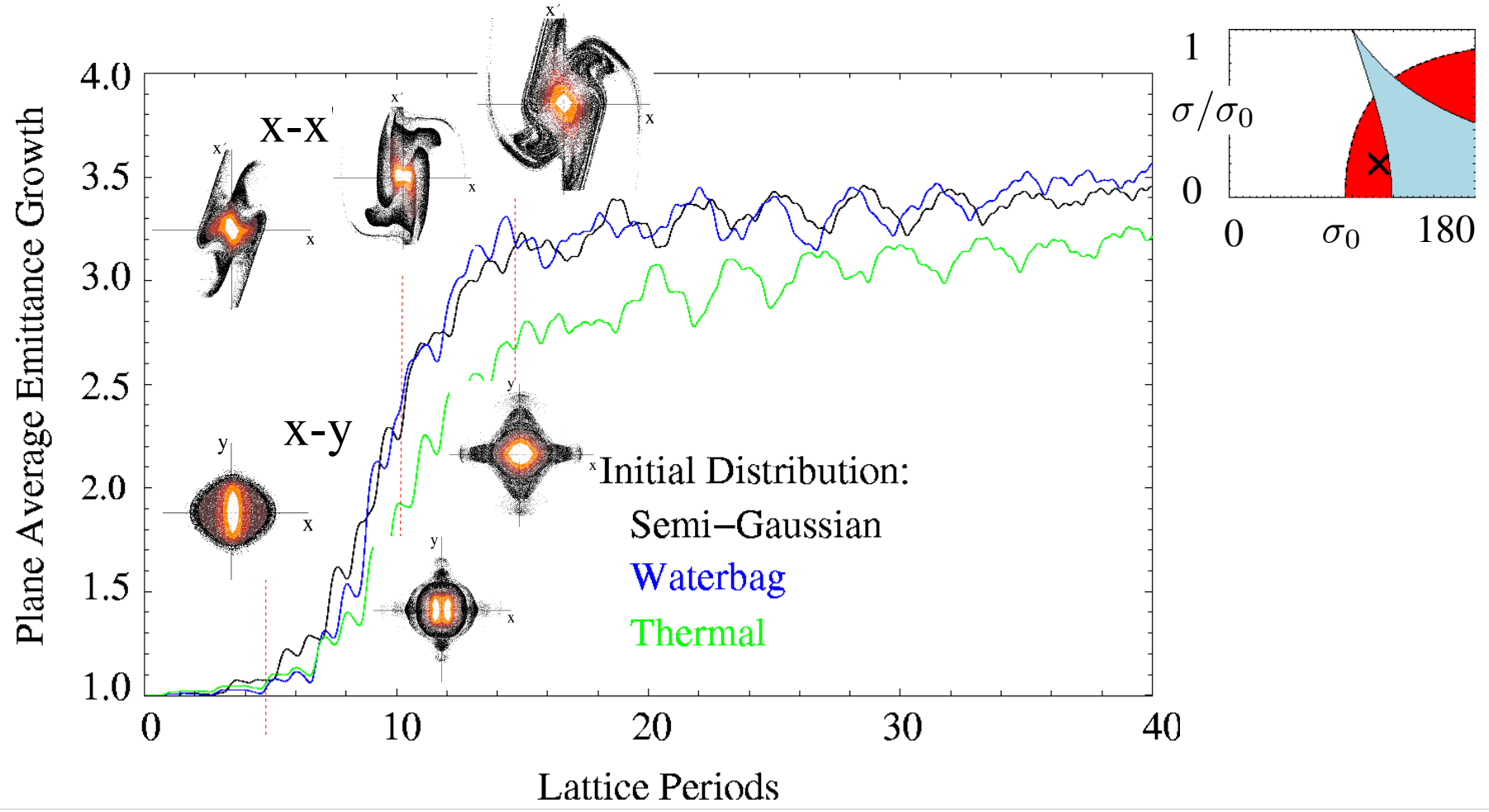

Self-consistent Poincare plots generated using Warp PIC simulations for cases of instability show large oscillation amplitude particles have halo-like resonant structure -- features insensitive to the initial distribution

Lattice period Poincare strobe

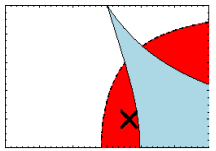

$$\sigma_0 = 110^\circ \quad \sigma/\sigma_0 = 0.2$$

Semi-Gaussian

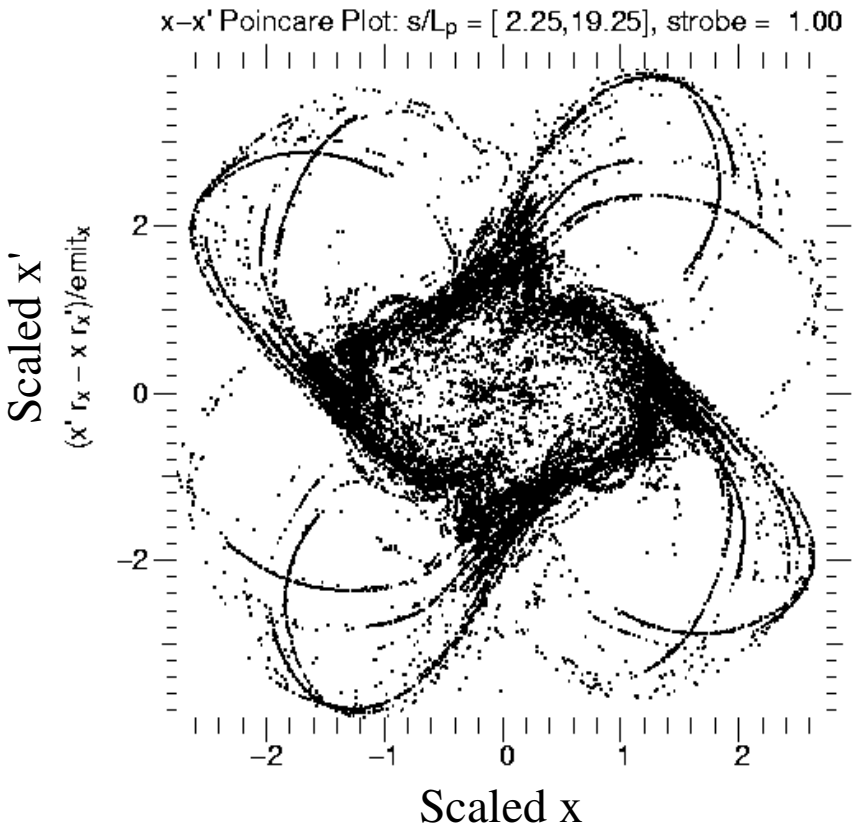

Thermal Equilibrium

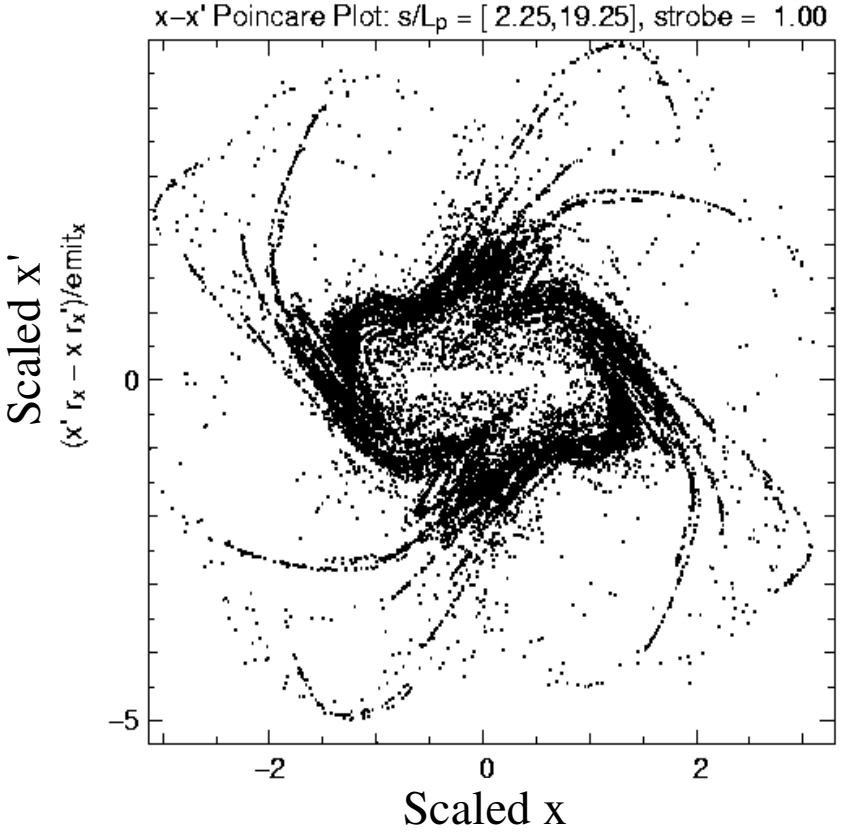

- Particles evolving along *x*-axis particles accumulated to generate clearer picture
  - Including off axis particles does *not* change basic conclusions

Extensive Warp PIC simulations carried out to better understand the parametric region of strong emittance growth

- Simulations advanced 6 undepressed betatron periods
  - Enough to resolve transition boundary: transition growth can be larger if run longer
- Strong growth regions of initial distributions all similar (threshold can vary)
  - Irregular grid contouring with ~200 simulations (dots) thoroughly probe instabilities

initial semi-Gaussian

- Initial thermal/Gaussian almost identical

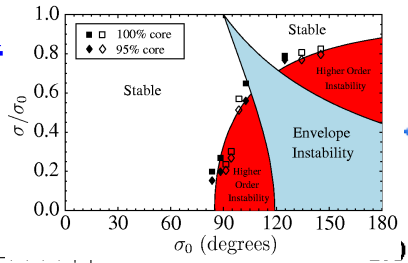

initial Waterbag

- Initial KV similar with extra unstable internal modes deep in stable region

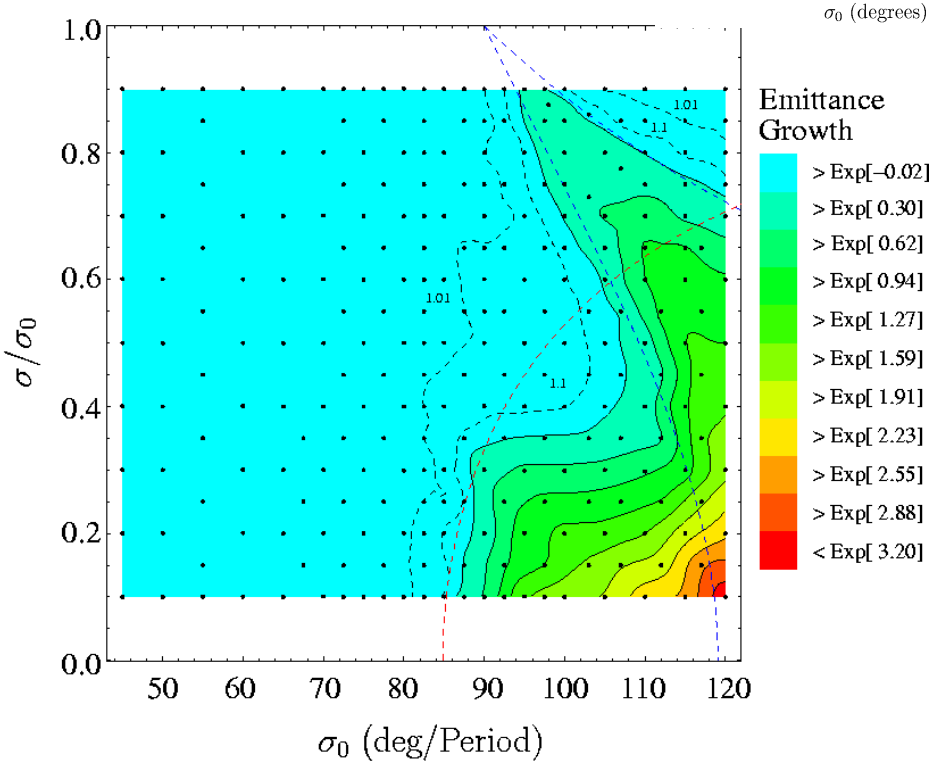

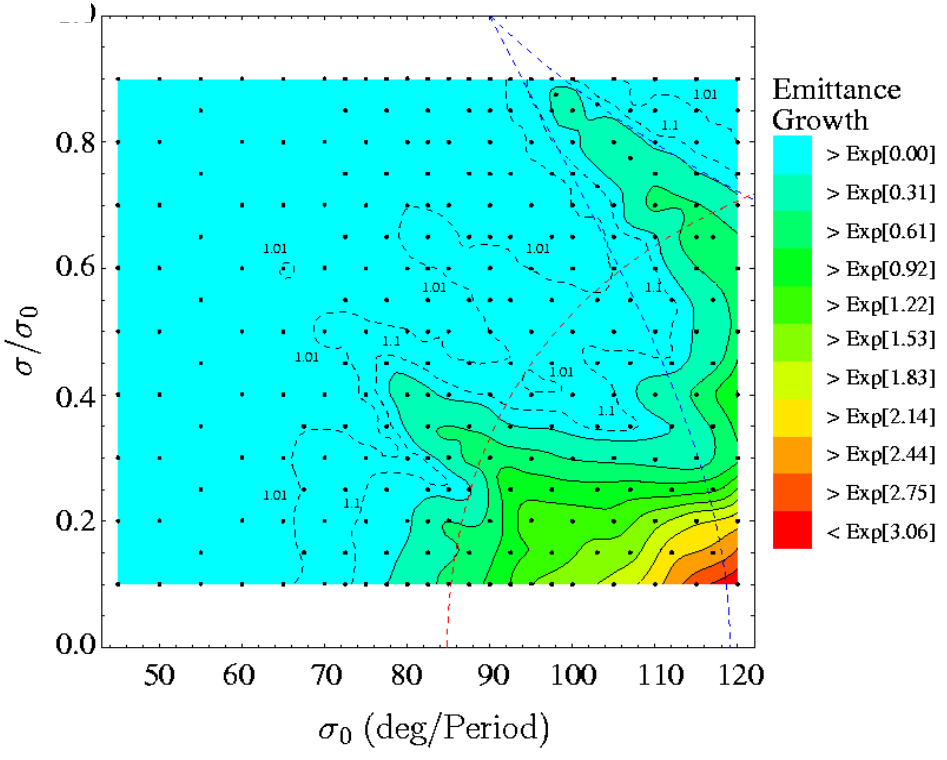

Core-Particle Model --- Envelope flutter at high focus strength and space-charge nonlinear forces drive strong resonances for particles evolving outside beam edge

Envelope (matched or mismatched) with actual flutter

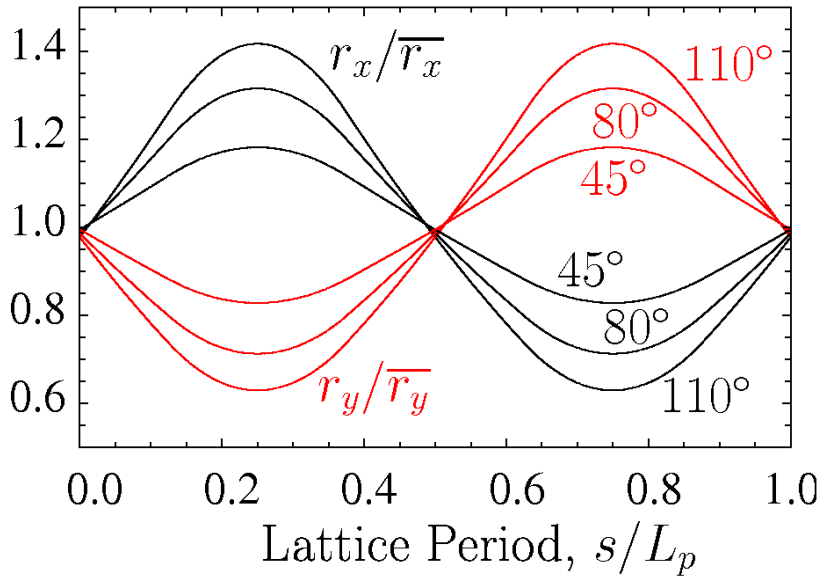

$$\overline{r_x} = \int_0^{L_p} \frac{ds}{L_p} r_x(s)$$

$\eta = 0.5 \quad L_p = 0.5$ m

$Q = 5 \times 10^{-4}$

$\varepsilon_x = \varepsilon_y = 50$ mm-mrad

σ_0	σ/σ_0
45°	0.20
80°	0.26
110°	0.32

Nonlinear force transition inside/outside uniform beam large for strong space-charge

- Illustrated for round beam

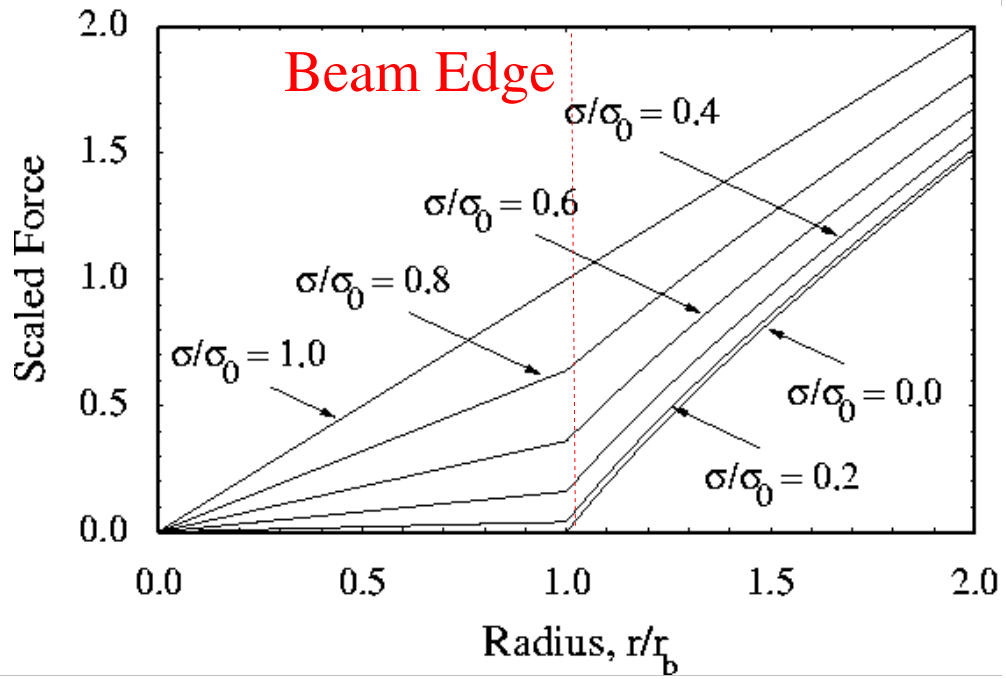

Core-particle simulations: Poincare plots illustrate resonances associated with higher-order halo production near the beam edge for FODO quadrupole transport

- High order resonances near the core are strongly expressed
- Resonances stronger for higher σ_0 and stronger space-charge
- Can overlap and break-up (strong chaotic transition) allowing particles launched *near the core* to rapidly increase in oscillation amplitude

Lattice Period Poincare Strobe, particles launched [1.1,1.2] times core radius

Stable

$\sigma_0 = 95^\circ, \quad \sigma/\sigma_0 = 0.67$

Unstable

$\sigma_0 = 110^\circ, \quad \sigma/\sigma_0 = 0.1$

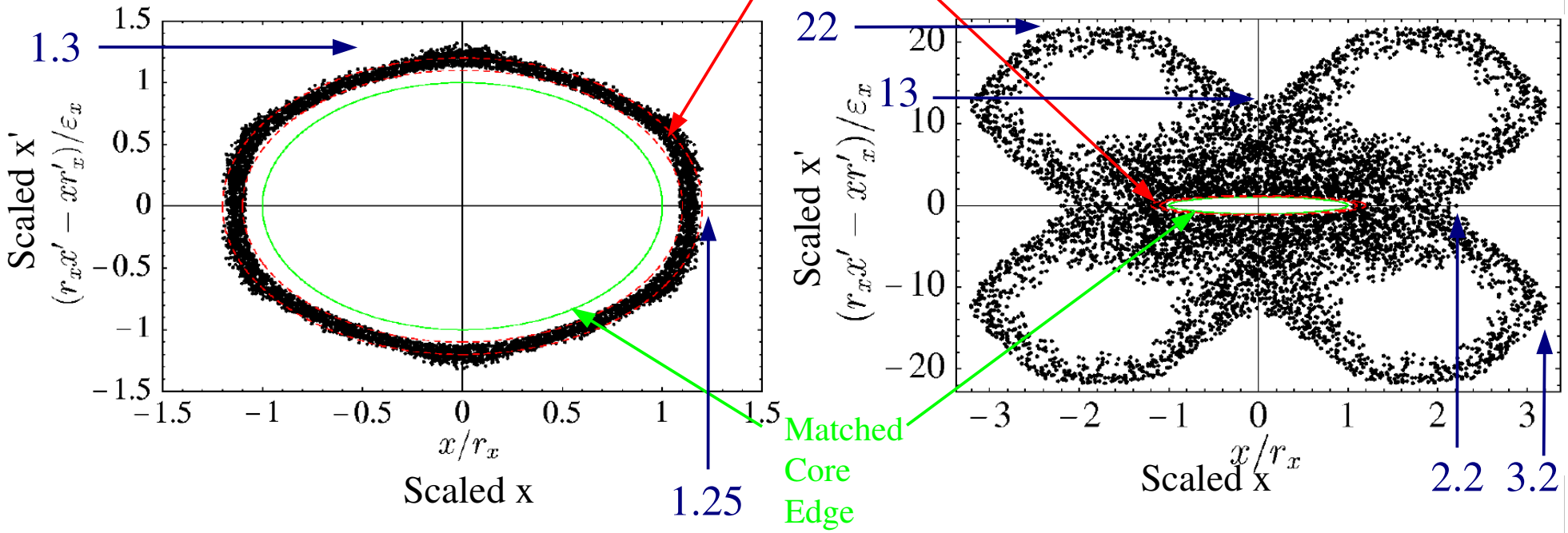

Core-particle simulations: Poincare phase-space plots illustrate stability regions where near edge particles grow in oscillation amplitude: launch [1.1,1.2]x core

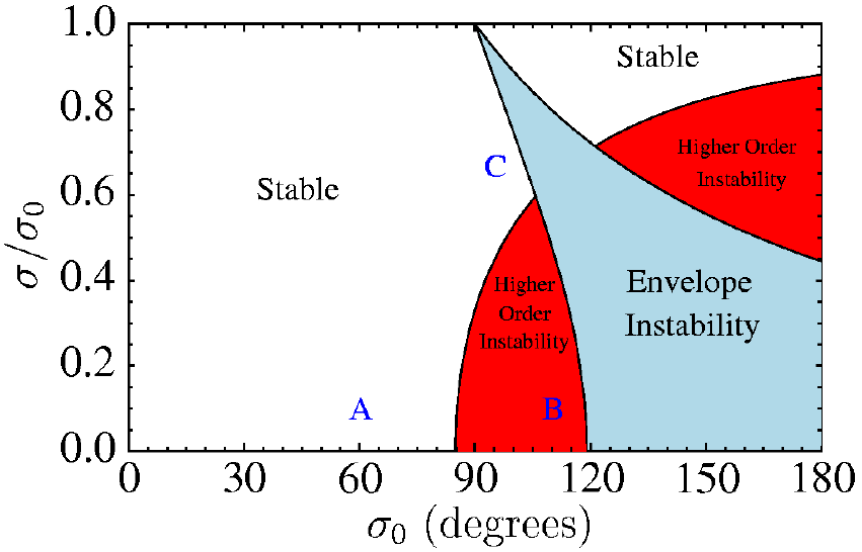

C (stable): $\sigma_0 = 95°,\ \sigma/\sigma_0 = 0.67$

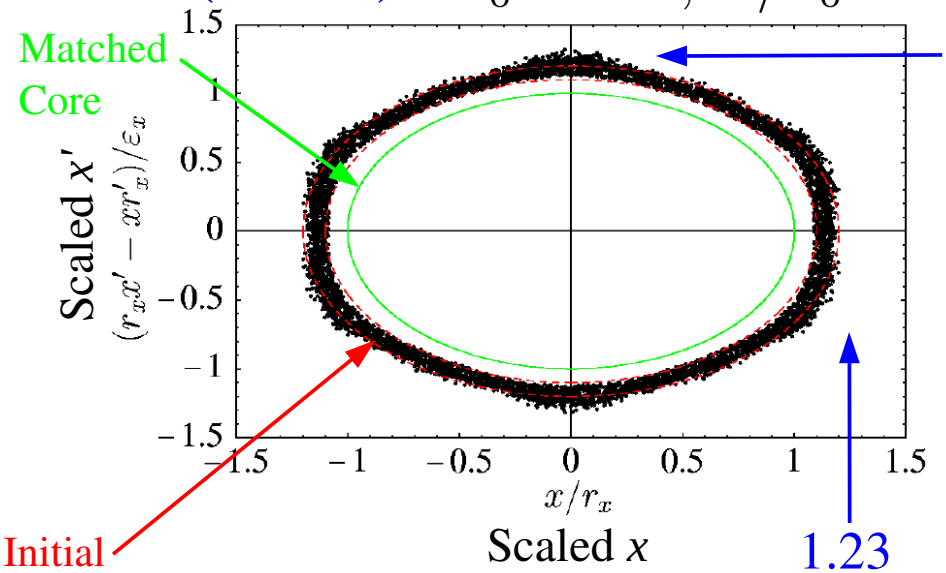

A (stable): $\sigma_0 = 60°,\ \sigma/\sigma_0 = 0.1$

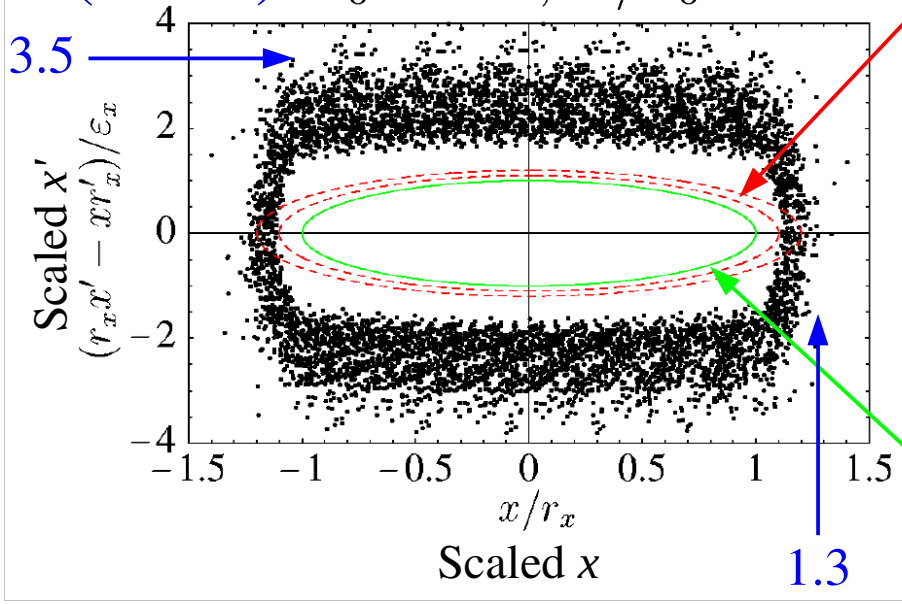

Range

B (unstable): $\sigma_0 = 110°,\ \sigma/\sigma_0 = 0.1$

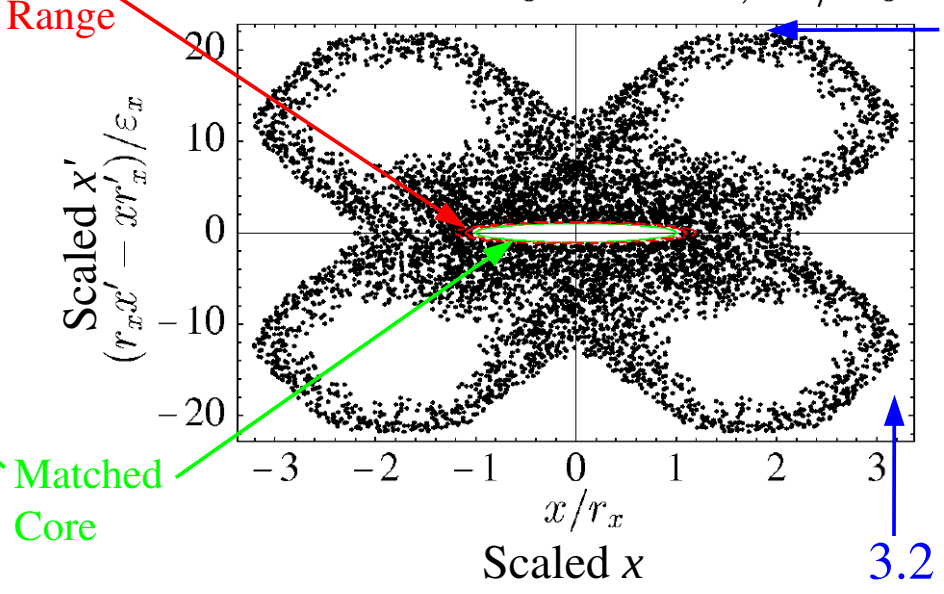

Contours of max particle amplitudes in core particle model suggest stability regions consistent with self-consistent simulations and experiment

Max amplitudes achieved for particles launched [1.05,1.1] times the core radius:

- Variation with small changes in launch position change picture little

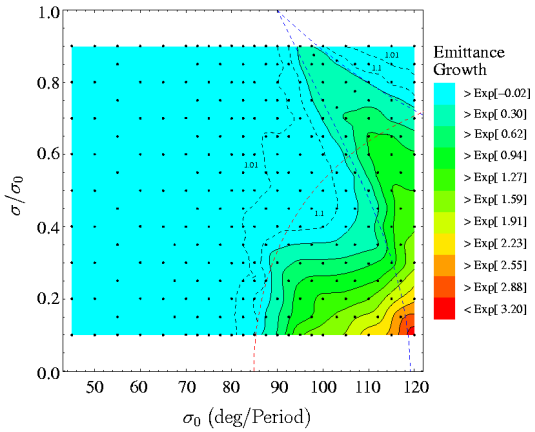

PIC Results

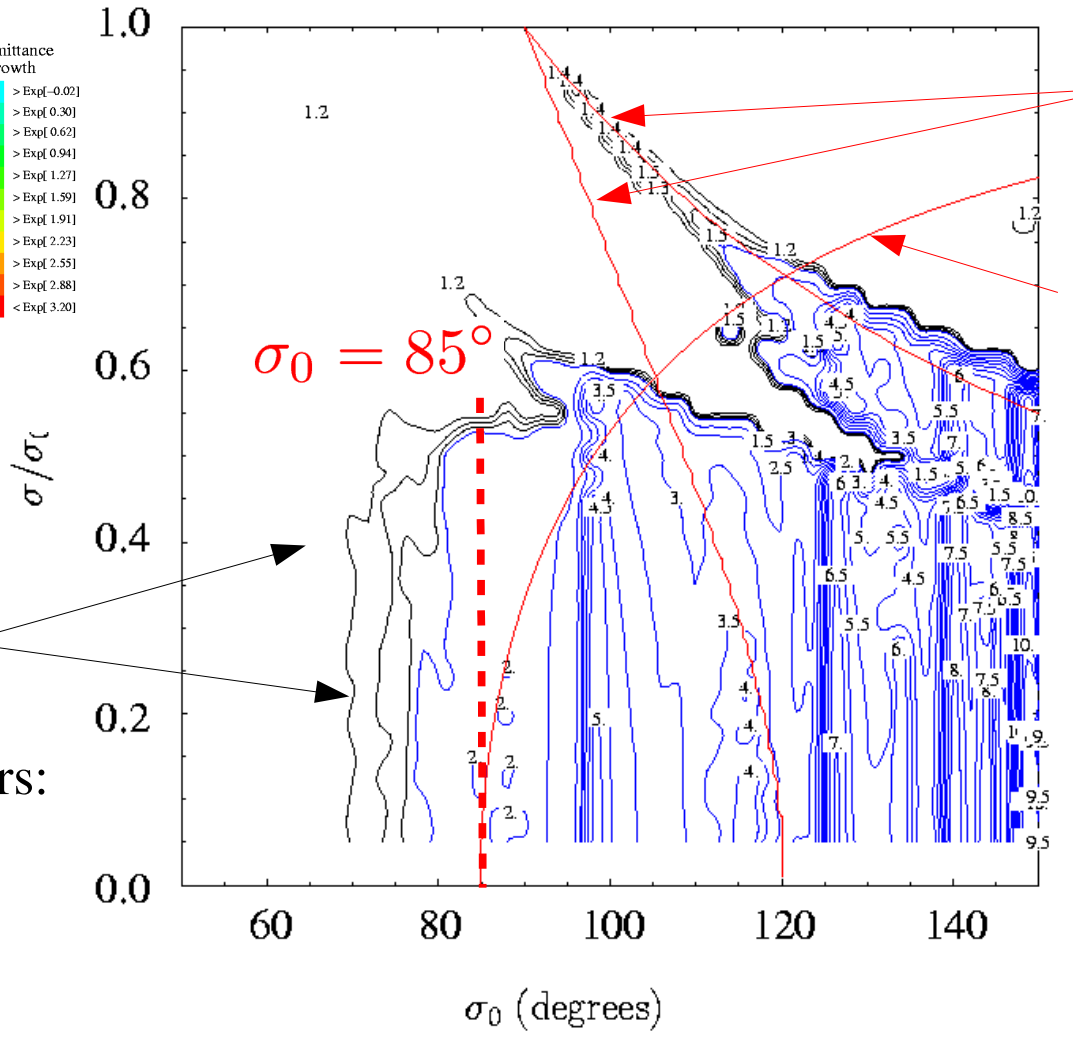

Envelope Band Edges

Tiefenback's curve fit to experimental stability boundary

Threshold Growth Black Contours: 1.2, 1.3, 1.4

Large Amplitude Growth Blue Contours: 1.5, 2.0, 2.5, ..., 10

Note: consistent with PIC results, instability well above envelope band not found

Discussion: Higher order space-charge stability limits in periodic quadrupole transport

High-order space-charge related emittance growth have long been observed in intense beam transport in quadrupole focusing channels with $\sigma_0 \gtrsim 85^\circ$

- SBTE Experiment at LBNL [M.G. Tiefenback, Ph.D Thesis, UC Berkeley (1986)]
- Original simulations by Haber, Laslett and parametric results by Lund, Chawla

A core-particle model developed show these space-charge transport limits result from a strong (non-tenuous) halo-like mechanism:

- Space-Charge and Envelope Flutter driven
- Results in large oscillation amplitude growth -- strongly chaotic resonance chain which limits at large amplitude rapidly increases oscillations of particles just outside of the beam edge
- Not weak: many particles participate -- Lack of core equilibrium provides pump of significant numbers of particles evolving sufficiently outside the beam edge
- Strong statistical emittance growth and lost particles (with aperture)

More details in comprehensive publications:

Lund, Chawla, NIMA 561, **203** (2006)

Lund, Barnard, Bukh, Chawla, Chilton, NIMA **577**, 173 (2007)

Lund, Kikuchi, Davidson, PRSTAB **12**, 114801 (2009)

Selected Topics on Space-Charge Effects in Intense Beams

1) US Particle Accelerator School and UC Berkeley courses on "Beam Physics with Intense Space-Charge"

2) Theory and numerical simulations on optimal Einzel lens transport

3) Multipole expansion for realistic modeling of focusing optics

4) Space-Charge induced transport limits in quadrupole focusing channels

5) Nonlinear focusing channel for stable beam transport and possible application to NGLS/APEX

Significant halo/distribution distortion observed on APEX injector for NGLS: Papadopoulous CBP Nov. Talk

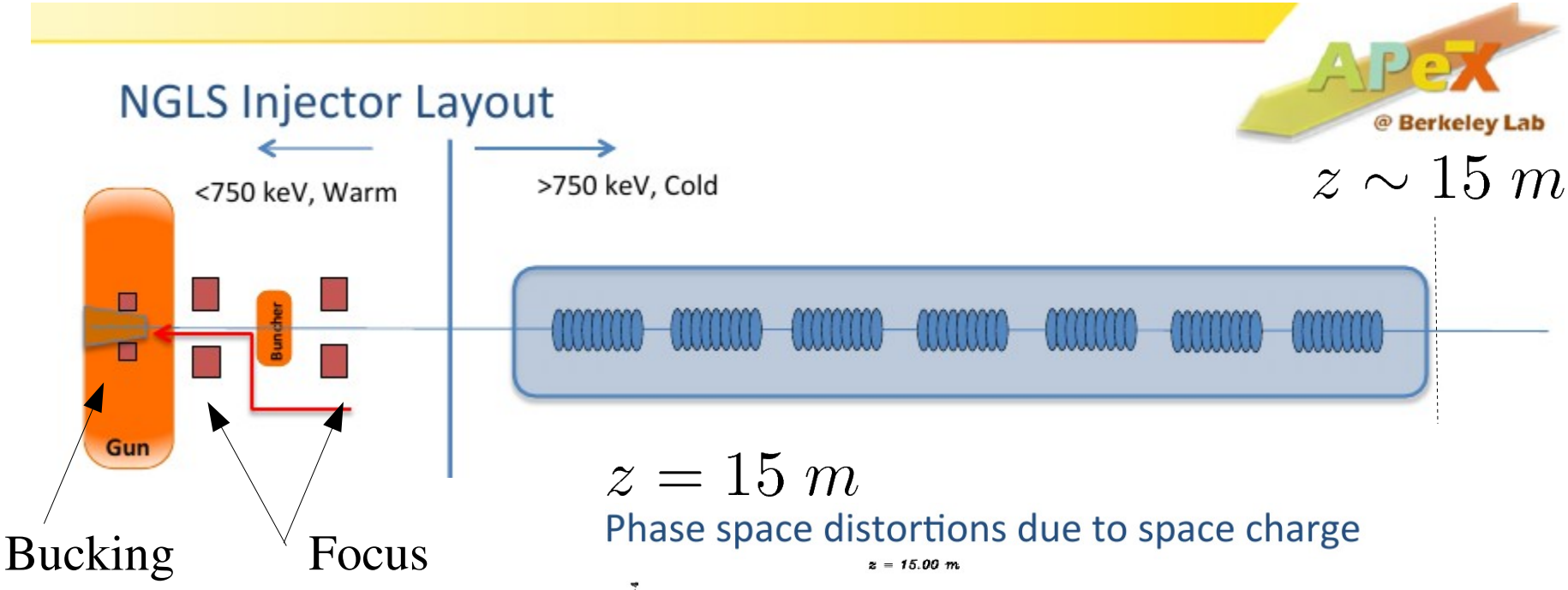

APEX @ Berkeley Lab

$z \sim 15\ m$

$z = 15\ m$

Phase space distortions due to space charge

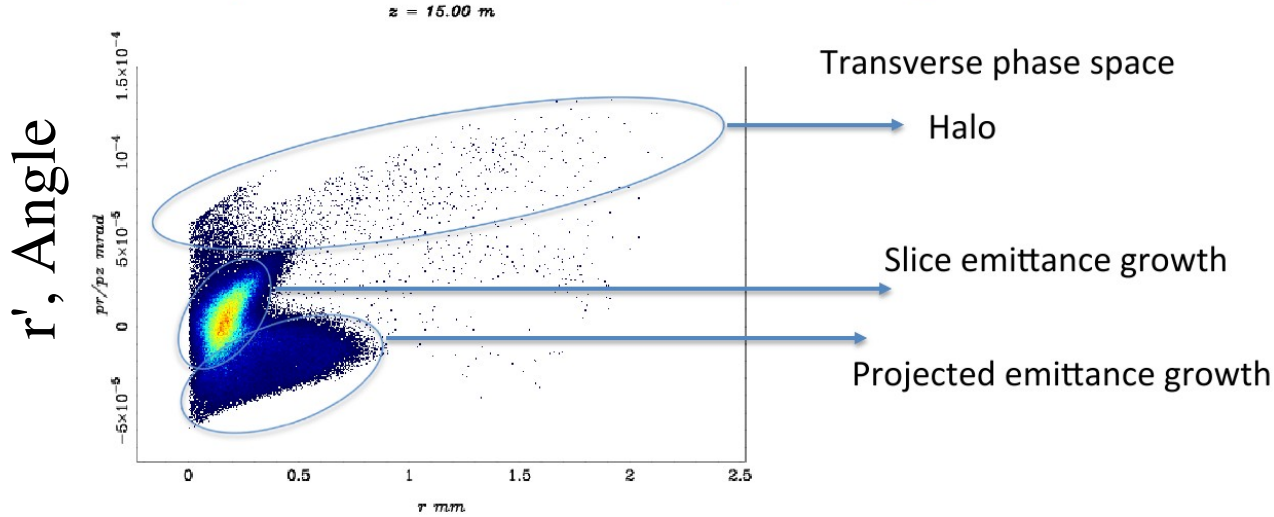

Basic Idea: Adjust applied focusing potential for linear beam dynamics with a stable distribution

Usual 2D Transverse Hamiltonian for continuous Linear Focusing:

$$H_\perp = \frac{1}{2}\mathbf{x}_\perp'^{\,2} + \frac{1}{2}k_{\beta 0}^2\mathbf{x}_\perp^2 + \frac{q}{m\gamma_b^3\beta_b^2c^2}\phi$$

$\Uparrow$ $\Uparrow$ $\Uparrow$

Kinetic — Applied Linear Focus — Self-Field: Generally nonlinear

$k_{\beta 0}^2 = \text{const}$: approx avg focus of periodic lattice

Use a nonlinear applied focus potential *V* for overall linear dynamics

$$H_\perp = \frac{1}{2}\mathbf{x}_\perp'^{\,2} + \underbrace{V + \frac{q}{m\gamma_b^3\beta_b^2c^2}\phi}$$

$$= \frac{1}{2}\mathbf{x}_\perp'^{\,2} + \qquad \frac{1}{2}k_{\beta 0}^2\mathbf{x}_\perp^2$$

$k_{\beta 0}^2 = \text{const}$: linear dynamics all particles

Procedure can be carried out with a manifestly stable thermal equilibrium beam distribution: Lund, submitted to NIMA, Dec. 2012

2D Vlasov-Poisson System for an unbunched beam

The sheet beam evolves in *x*-*x*' phase-space according to Vlasov's equation:

$$\left\{ \frac{\partial}{\partial s} + \frac{\partial H}{\partial \mathbf{x}'_\perp} \cdot \frac{\partial}{\partial \mathbf{x}_\perp} - \frac{\partial H}{\partial \mathbf{x}_\perp} \cdot \frac{\partial}{\partial \mathbf{x}'_\perp} \right\} f(\mathbf{x}_\perp, \mathbf{x}'_\perp, s) = 0$$

with

$$H_\perp = \frac{1}{2} {\mathbf{x}'_\perp}^2 + V + \frac{q}{m\gamma_b^3 \beta_b^2 c^2} \phi$$

and coupling to the field specified by Poisson's equation

$$\left(\frac{\partial^2}{\partial x^2} + \frac{\partial^2}{\partial y^2} \right) \phi = -\frac{q}{\epsilon_0} n$$

$$n = \int d^2\mathbf{x}'_\perp \; f_\perp$$

$$\phi(\mathbf{x}_\perp = 0) = 0$$

Apply procedure to a thermal beam distribution

Analysis of the rest frame transformation shows that the 2D Maxwell-Boltzmann distribution (lab frame temperature definition) is:

$$f_\perp(H_\perp) = \frac{\beta n_0}{2\pi}\exp\left(-\beta H_\perp\right)$$

$$n_0 = n(\mathbf{x}_\perp = 0)$$

$$\beta \propto \frac{1}{T} = \text{const}$$

- Temperature uniform spatially

$$T_x \equiv \gamma_b m \beta_b^2 c^2 \frac{\int d^2x'\ x'^2 f_\perp}{\int d^2x'\ f_\perp} = \frac{m\gamma_b\beta_b^2 c^2}{\beta} = T = \text{const}$$

- Density nonuniform: solve Poisson equation to calculate
  - Structure depends on applied focus V and space-charge intensity
- Manifestly stable by distribution concavity: Fowler, Davidson

$$\frac{df_\perp(H_\perp)}{dH_\perp} \leq 0 \quad \Longleftrightarrow \quad \text{Sufficient condition for stability}$$

- Parameters: eliminate theory parameters to accelerator relevant and express in terms of a uniform density rms equivalent KV beam.

$$\left.\begin{array}{l} n_0 \\ \beta \\ k_\beta \end{array}\right\} \Longrightarrow \left\{\begin{array}{ll} Q & \text{Perveance} \\ \varepsilon_{\text{rms},x} & \text{rms x-emittance} \\ \sigma_x & \text{Density profile extent (sigma)} \end{array}\right\} \quad \sigma/\sigma_0 \in [0,1] \quad \text{Tune depression of rms equivalent beam}$$

Review: for linear focusing stable beam has highly nonlinear dynamics

Lund, Kikuchi, Davidson, PRSTAB 2009

$Q = 10^{-4}$ $\quad k_{\beta 0}^2 = \text{const}$

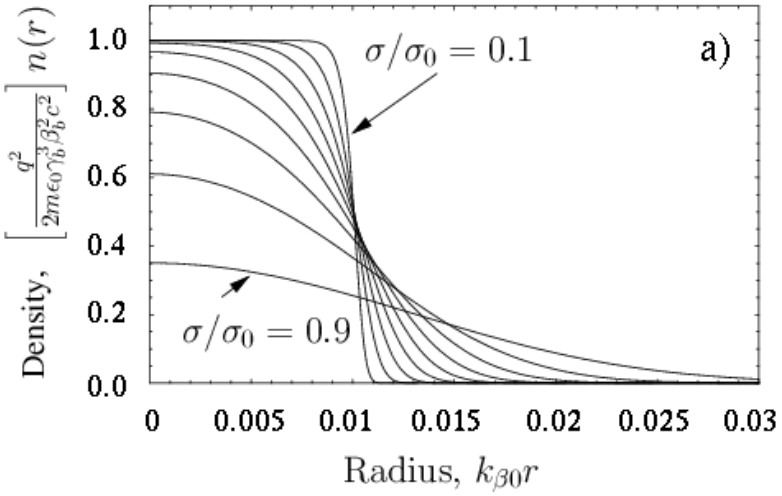

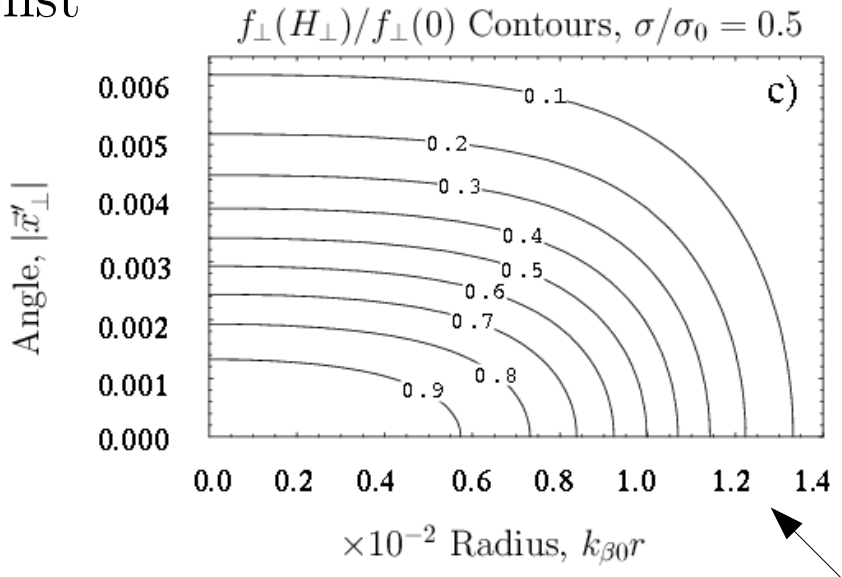

Radial scales change

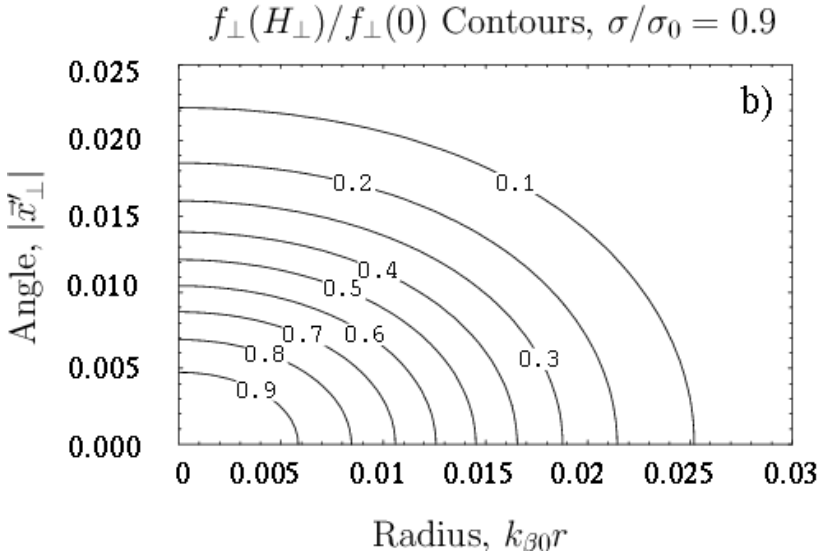

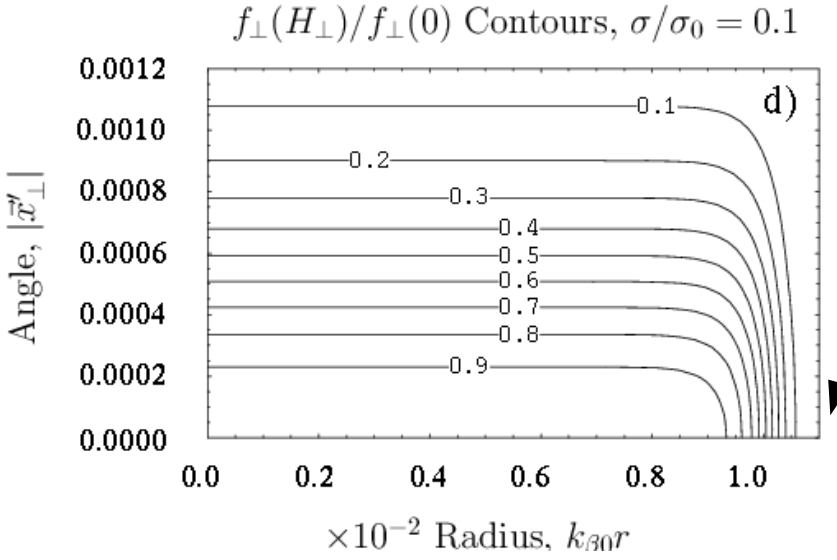

Nonlinear Focusing

Density Profile always Gaussian:

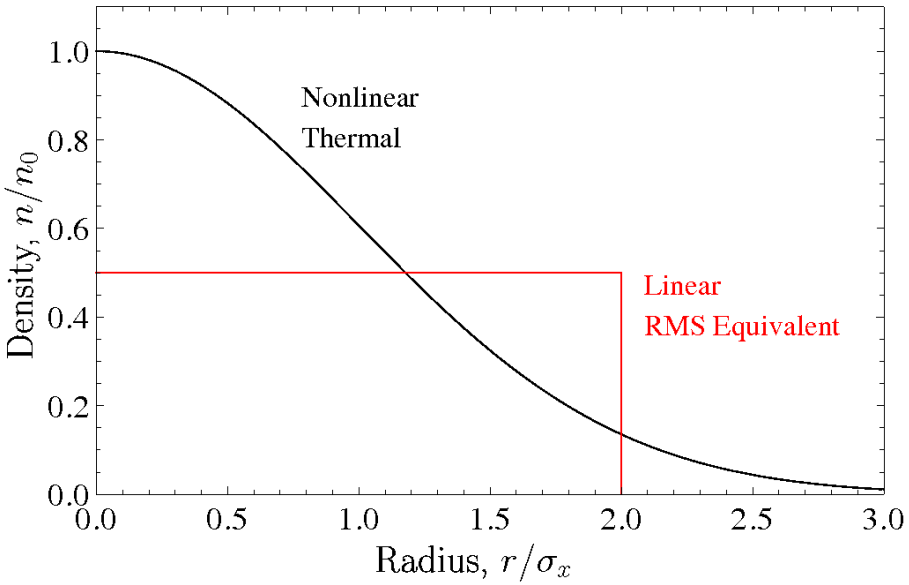

Applied Focus Potential *V*:

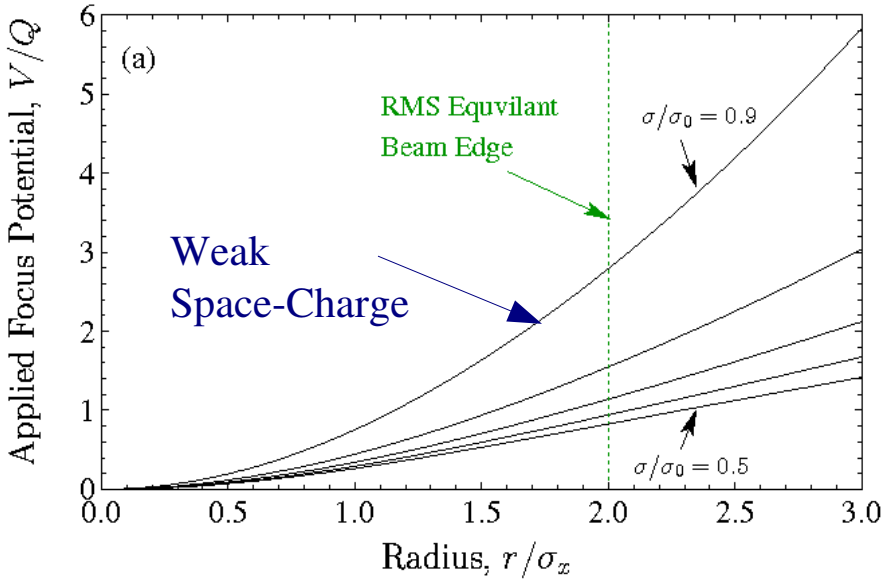

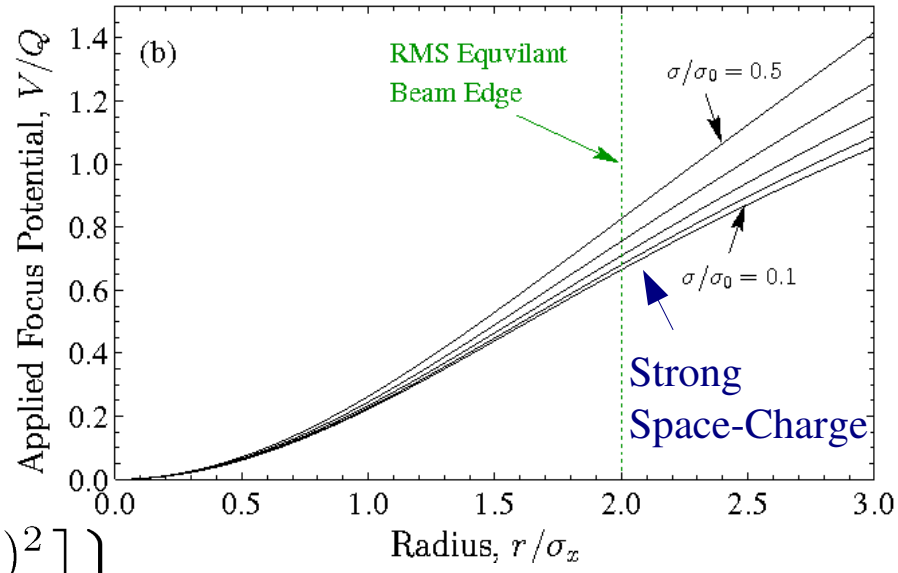

Closed-form solution for *V*:

$$V = \frac{Q}{8}\frac{(\sigma/\sigma_0)^2}{1-(\sigma/\sigma_0)^2}(r/\sigma_x)^2 + \frac{Q}{2}\left\{\gamma_E + \log\left[\frac{(r/\sigma_x)^2}{2}\right] + E_1\left[\frac{(r/\sigma_x)^2}{2}\right]\right\}$$

Properties of Nonlinear Focusing Potential

Focus Strength relative to linear focus strength for rms equivalent beam

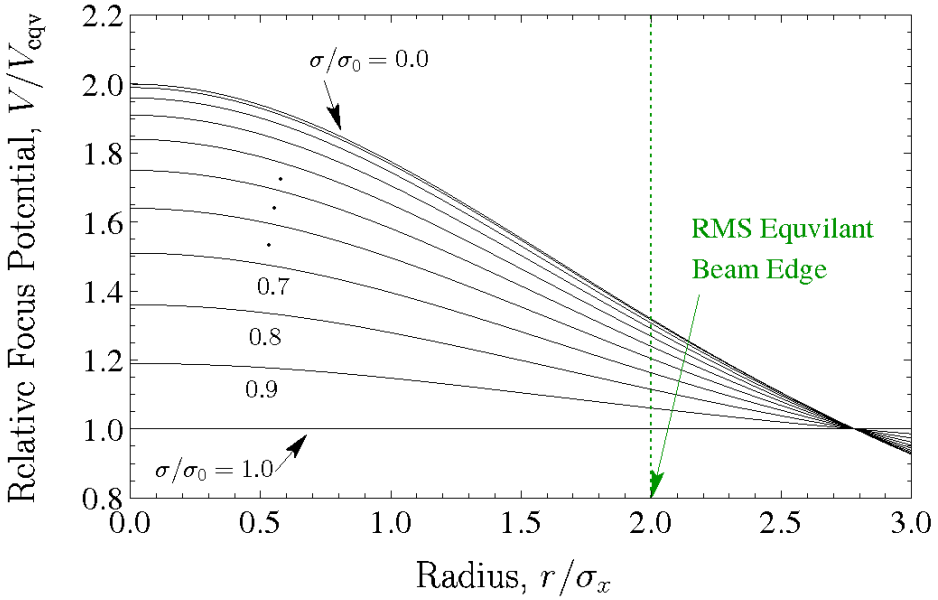

$$V \rightarrow V_{\mathrm{eqv}} = \frac{1}{2} k_{\beta 0}^2 r^2$$

Multipole structure of nonlinear focus $V = \sum_{n=1}^{\infty} V_n \left(\frac{r}{\sigma_x} \right)^{2n}$

n => 2n-pole multipole equivalent

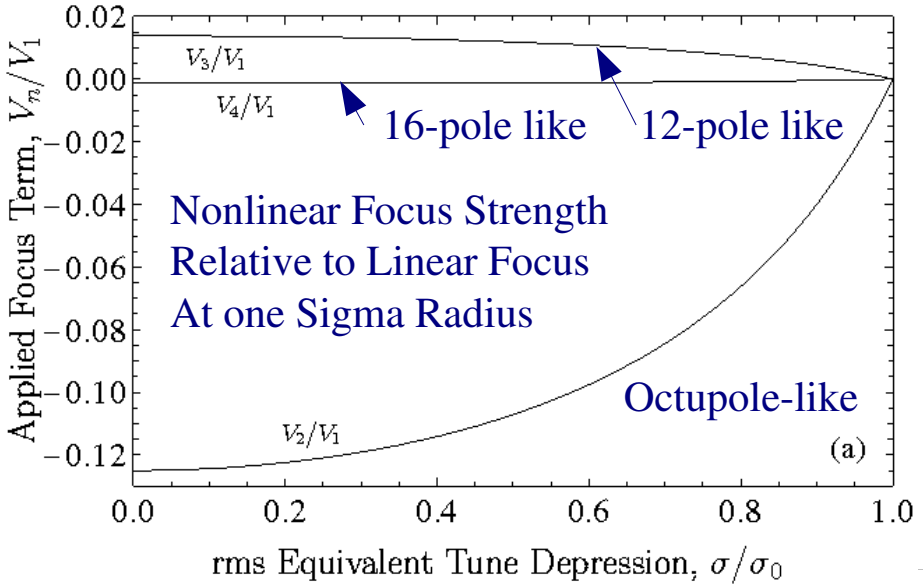

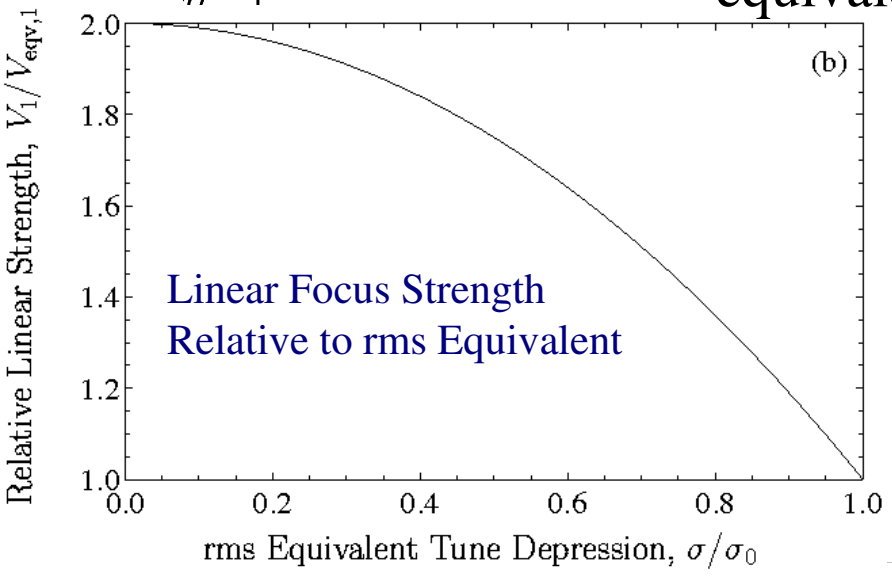

Discussion on application to NGLS/APEX

- Nonlinear focus could maintain distribution force balance from Gaussian injection with strong space-charge to suppress generation of halo
  - Provides extra/better "knob" to optimize better than just linear focus
  - Nonlinear fields small and can be rapidly decreased with acceleration to transition to a linear lattice as space-charge becomes weak
  - Results apply to "chopped" Gaussian also (field outside beam arb though)
- More work necessary to evaluate if practical
  - Real beam periodic focused and very short axially
  - Need to characterize effective nonlinear focus strength of AG multipoles
- Possible Path to evaluate:
  1) Simulate idealized (fictitious) field superimposed on realistic (present) APEX lattice model to see if improvements can be realized
  2) Design nonlinear focus to approximate idealized nonlinear focus force
     Electric Multipole? Magnetic Multipole?
  3) Simulate realistic lattice model to evaluate whether significant gains realizable and implement if promising

Conclusions

Topics Overviewed:

1) US Particle Accelerator School on "Beam Physics with Intense Space-Charge"
2) Theory and numerical simulations on optimal Einzel lens transport
3) Multipole expansion for realistic modeling of focusing optics
4) Space-Charge induced transport limits in quadrupole focusing channels
5) Nonlinear focusing channel for stable beam transport and possible application to NGLS/APEX

Additional topics not covered:

- Lattice design
- Beam steering and control
- Equilibrium beam structure
- Debye screening
- Envelope modes
- Collective instabilities
- Beam Halo: transverse and longitudinal
- Dispersion effects with space-charge
- Bunch compression in rings
- Diagnostic development
- Low dimensional models

⋮

- Numerical Simulations
- Warp code for intense beam modeling
- Modeling transport experiments
- Distribution Loading
- Bunch end blowoff
- Effective length of focusing optics
- Magnetic optics: Permanent and superconducting
- Electric optics: Dipoles, Quadrupoles
- Magnetic pinch focusing
- Paul Trap modeling of long-path length beam transport

⋮